Master of Science Thesis

Finite Element Analysis of Spudcan Penetration in Homogeneous and Two Layered Soil Deposits

Anandro Amellonado

October, 2016

TU Delft

MSc. Offshore and Dredging Engineering (ODE) – Bottom Founded Offshore Structure Track

Finite Element Analysis of Spudcan Penetration in Homogeneous and Two Layered Soil Deposits

By

Anandro Amellonado
Student id: 4348141

in partial fulfilment of the requirements for the degree of

Master of Science

in Offshore and Dredging Engineering

at the Delft University of Technology,

to be defended on 21st October, 2016

Thesis committee:
Prof. Dr. A. V. Metrikine, TU Delft
Dr. F. Pisanò, TU Delft
Ir. J. S. Hoving, TU Delft
Dr. M. Alvarez Grima, IHC MTI
Ir. T. Wambeke, IHC MTI

TU Delft

This thesis is sponsored by IHC MTI. Their contribution is hereby acknowledged.
Cover photo courtesy of IHC MTI

Summary

Mobile jack-up units remain favourable in the offshore industry due to its capability to self-install and ability to work in moderate water depth. Prior to its mobilization to the site location, it is required to have a site-specific assessment (SSA). The SSA will identify any potential problems related to foundation conditions during installation. One of the important site specific assessments before deploying jack-up units is the preload check, which is carried out to predict the load-penetration response. The offshore industry has published the 'Guidelines for the Site Specific Assessment of Mobile Jack-Up Units' (SNAME 2008) and more recently, the International Standard Organization has published ISO 19905-1: 2012 in order to standardize jack-up assessment procedures. The guidelines adapt the framework used for onshore application following conventional bearing capacity theory to assess spudcan penetration depth.

However, these guidelines are limited in discussing the approach in working in multi-layered soils. The conventional procedures described in the guidelines may not be sufficiently accurate since the methods cannot take a proper account of the nature of continuous spudcan penetration process. In practice, a layered system is commonly encountered and the installation process can be hazardous, with the potential of punch-through failure when the spudcan penetrates into strong over weak materials. A better understanding is therefore required. This thesis proposes that an analysis based on numerical modelling can be one possible alternative in evaluating spudcan bearing capacity in the layered system.

This study presents the application of a finite element modelling approach, called Press-Replace (PR) Technique, which is based on a small strain geometry update procedure. This technique can be applied in any geotechnical software that is currently available for engineering practice. The PR Technique is employed to investigate the performance of penetrating spudcan foundations on homogeneous soil (sand and clay) and two layered soil deposits (sand overlying clay). The numerical method is firstly verified against previous experimental and numerical test data. A parametric study is also conducted to see the influence of normalized soil properties and geometry on the load penetration curves.

Overall, the modelling approach used in the present study shows a good agreement, compared to other published results. The PR Technique shows its capability to simulate the penetrating spudcan foundations. In addition, several interesting findings are identified based on the parametric study: (i) the *stress-level-effect* and the prominent influence of dilatancy angle on the spudcan penetration in sand; (ii) the difference of soil flow mechanism in clay that leads to the attainment of the bearing capacity factor in deep penetration; and (iii) the onset of punch-through in double layered case that is highly determined by the sand thickness ratio.

Lastly, some design charts are presented for all the investigated cases in the present study. These charts might be used to generate full spudcan bearing resistance-depth curves in sand, clay and sand overlying clay.

Keyword: Spudcan, bearing resistance, load penetration response, layered soil deposits, punch-through, PR Technique, geometry update.

Acknowledgement

I would like to express my gratitude to my committee members:

Prof. Metrikine, the committee chairman, for his valuable comments in all the progress meetings I had, and also for the personal statement he gave to my academic counsellor so that I could get the graduation support scheme.

Federico Pisanò, my daily supervisor, who consistently steered me in the right direction and gave valuable feedback. He always found time to answer my email even in his busy time in Australia.

IHC MTI, especially for my company supervisors Tom and Mario, thank you for giving me the opportunity to learn and work on this interesting thesis topic. I really appreciate all the fruitful discussions we had during my time at MTI.

Furthermore, I would like to thank Kürşat Engin. I wouldn't be able to finish my thesis without the methodology you introduced. Thank you for being interested in my thesis and providing many comments and literatures.

Faraz Tehrani, Neyamat Ullah, PLAXIS Help Desk, and PLAXIS Users group for solving my queries.

I would like to thank my parents and my brother for their continuous support and prayer. Lastly, thanks to all my friends who made my life in The Netherlands more colourful.

Anandro Amellonado

Table of content

List of Figures

List of Tables

List of symbols

A	Spudcan area at maximum diameter
B	Spudcan diameter at largest section
B^T	Matrix containing the derivatives of the shape functions
B_{BD}	Bottom boundary distance
D	Spudcan diameter at largest section
E	Young modulus
E_i	Interface Young modulus
E_{soil}	Young modulus of the surrounding soil
E_{oed}	Oedometric stiffness
$E_{oed,i}$	Interface oedometric stiffness
G	Soil shear modulus
G_i	Interface shear stiffness
H	Horizontal load
H_s	Sand thickness
H_{cav}	Open cavity depth
K	Stiffness matrix
K_s	Punching shear coefficient
L_{BD}	Lateral boundary distance
M	Moment load
N_c	Bearing capacity factor due to cohesion
$N_{c,pp}$	Post peak bearing capacity factor (in the underlying clay layer)
N_{c0k}	Bearing capacity factor for spudcan on non-homogeneous clay
$N_{c0\alpha}$	Contribution of the normal stress on the cone face of the spudcan
N_{cd}	Deep bearing capacity factor for spudcan penetation on clay

N_q	Bearing capacity factor due to surcharge
N_γ	Bearing capacity factor due to unit weight of soil
Q_v	Ultimate vertical foundation capacity
$Q_{u,b}$	Fictitious footing's capacity
R	Spudcan radius
R_{inter}	Soil - spudcan interface reduction factor
R_{sc}	The strength ratio of sand to clay
V_0	Maximum vertical load capacity when H=0 and M=0
V_{0m}	Peak value of V_0 in the strain hardening law
W	the weight of the sand between the spudcan and fictitious footing
c	Cohesion
c_i	Cohesion of the interface
c_{soil}	Cohesion of the surrounding soil
d	Spudcan penetration depth
d_{peak}	Depth of peak penetration resistance
d_c	Depth factor for bearing capacity factor due to cohesion
d_q	Depth factor for bearing capacity factor due to surcharge
d_γ	Depth factor for bearing capacity factor due to self-weight
f	Yield function
f_p	Initial plastic stiffness factor
g	Plastic potential fucntion
h_{plug}	Thickness of sand plug
i	Step
j	Stress exponent
k	Gradient of undrained shear strength

k	initial plastic stiffness
m	modulus number
n_s	Load spread factor
ph	Phase
q	Bearing pressure
q_c	Bearing pressure in clay
q_{peak}	Peak bearing pressure
q_o	Effective overburden pressure
q_u	Ultimate bearing capacity
s_c	Bearing capacity shape factor
s_{fp}	New constant factor for calculating vertical load capacity
s_u	Undrained shear strength
s_{uH}	Undrained shear strength at the limiting cavity depth
s_{um}	Undrained shear strength at the mudline or at the sand-clay interface for double layered system
s_{u0}	Undrained shear strength at the footing base level
t_s	Slice thickness
u	Displacement
u_y	Prescribed displacement/ step size (= penetration length)
w	Vertical footing displacement
w_p	Plastic vertical footing displacement
p'_o	Effective overburden pressure
α	Interface roughness coefficient
β	Cone apex angle
γ'	Effective unit weight of soil
γ'_c	Effective unit weight of clay

γ'_s	Effective unit weight of sand
ΔF_y	The applied load on the footing
ΔF_x	The horizontal nodal forces
Δ_f	Load increment
Δ_u	Displacement increment
Δ_u	The horizontal displacement
Δ_v	The vertical dispalcement
δ	Dissipation parameter
δ_p	Dimensionless plastic penetration at peak
ε	Strain
ε^e	Elastic strain
ε^p	Plastic strain
ρ	Gradient of undrained shear strength
σ'	Effective stress
σ_r	Reference stress
$\sigma^{i,o}$	Stress state at the beginning of phase *i*
φ	Friction angle
φ^*	Reduced friction angle caused by non-associated flow
ν	Poisson's ratio
ν_i	Interface Poisson's ratio
ψ	Dilatation angle

Abbreviations

AEL	Arbitrary Eularian-Lagrangian
BD	Boundary Distance
CEL	Coupled Eularian-Lagrangian
CPT	Cone Penetration Test
FE	Finite Element
ISO	International Standard Organization
JIP	Joint Industry-funded Project
LB	Lower Bound
LDFE	Large Deformation Finite Element
MPM	Material Point Method
PIV	Particle Image Velocimetry
PR	Press-Replace
RD	Relative density
SNAME	The Society of Naval Architects and Marine Engineers
SSFE	Small Strain Finite Element

Chapter 1.
Introduction

1.1 Introduction to the problem

The jack-up or self-elevating unit is a mobile platform consisting of a buoyant hull fitted with movable legs, capable of raising its hull over the sea surface. They have been used for installation works as can be seen in Figure 1-1, fixed platform work-over, and for production support. Like a jacket structure or gravity-based structure, the jack-up offers a steady working platform. Mobile jack-up units remain favourable due to its capability to self-install and ability to work in moderate water depth.

Figure 1-1 Jack-up unit for wind turbine installation ("Royal IHC," 2016).

The great majority of self-elevating units in the world have either three or four legs. Each of the legs of the jack-up unit is normally supported on the sea floor via spudcan or mats. The geometry of the spudcan is typically hexagonal or octagonal in plan with a shallow conical underside and a sharp protruding spigot. The spudcan of large jack-up units nowadays can be up to 20m of diameter with various shapes while smaller legged jack-up may only have tubular legs. While the other type, the mat-supported jack-up rig, has fallen into disfavour because it can only work on a relatively even seabed of soft soils. Figure 1-2 shows some examples of spudcan configurations.

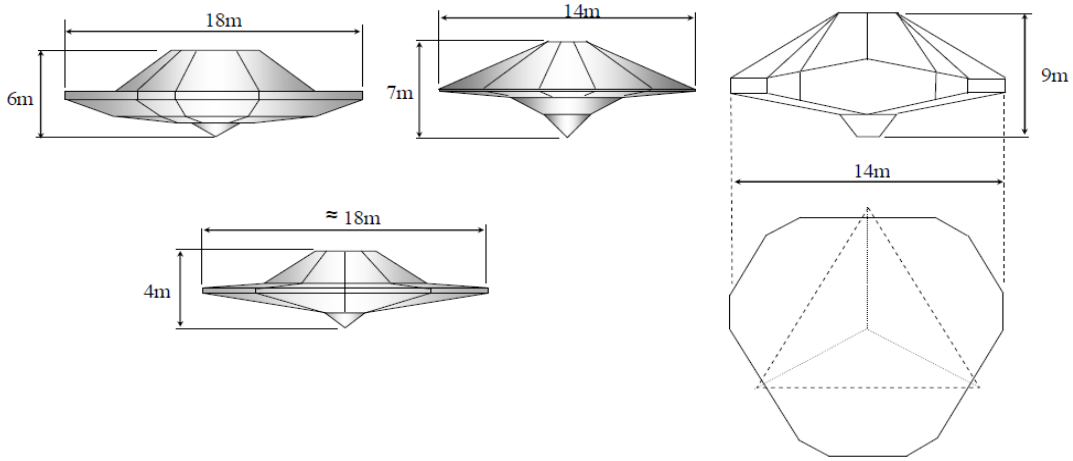

Figure 1-2 Some examples of spudcan geometries (Teh, 2007).

In the operational modes, tug boats firstly tow the self-elevating unit to the desired offshore location. Then the unit is jacked to be lifted clear of the water before preloading takes place. The preloading process is done by pumping water ballast on board in order to ensure adequate bearing capacity is achieved, so that the offshore operations can be done safely. Vertical loading, self-weight of the jack up and the water ballast, dominates during preloading process and is assumed to act directly through the centre of the conical footing. Following which, the ballast tank will be emptied before the operations start.

It would be important to note that jack-up units are not designed for only one specific offshore site. With the variety of offshore soils throughout the world, different soil properties, behaviour, and classification, it is therefore required to have a site-specific assessment (SSA) prior to every mobilization. The SSA will identify any potential problems related to foundation conditions during installation, operation and extraction. One of the important site specific assessments before deploying jack-up unit is the preload check, which is carried out to predict the load-penetration response. This check takes into account the geometry of the spudcan, soil model, designed soil profile, and the maximum preload of each spudcan.

According to InSafeJIP 2011, the purposes of this load-penetration prediction are:

- To establish whether the rig may be able to operate at the site.
- To identify any potentially hazardous conditions so that plans can be made to mitigate risks.
- To provide a benchmark against which the actual load-penetration performance can be compared. In this case, if the deviations from the predictions occur, it may indicate that there is an inadequate understanding of ground conditions.

The offshore industry has published the 'Guidelines for the Site Specific Assessment of Mobile Jack-Up Units' (SNAME 2008) and more recently, the International Standard Organization has published ISO 19905-1: 2012 in order to standardize jack-up assessment procedures. The guidelines adapt the framework used for onshore application following conventional bearing capacity theory to assess spudcan penetration depth. The vertical bearing capacity of the spudcan foundation is evaluated considering a number of possible depths, so called "wished-in-place" method, see Figure 1-3, and then the penetration curve is progressively constructed from independent calculations at different depths.

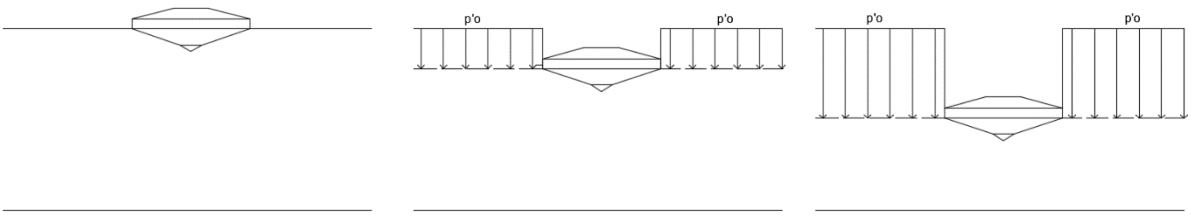

Figure 1-3 "wished-in-place" method.

However, these guidelines are inadequate in advising the approach to multilayered soils. The conventional procedures described in the guidelines may not be sufficiently accurate since they cannot take proper account of the nature of continuous spudcan penetration process. In practice, the layered system is commonly encountered and the installation process can be hazardous, with

the potential of punch-through failure when spudcan penetrates into strong over weak materials. This failure event may result in rig damage, such as buckling of the legs and lost drilling time (Cassidy et al., 2015). A better understanding is therefore needed and analysis based on numerical modelling can be one possible alternative option to evaluate spudcan bearing capacity in layered system. Furthermore, large deformation numerical analysis such as Arbitrary Eularian-Lagrangian (AEL), Coupled Eularian-Lagrangian (CEL), and most recently Material Point Method (MPM) would be required in order to correctly model continuous penetration. Nevertheless, these methods are not yet generally available or common for engineering applications (Engin et al., 2015) and are considered beyond the scope of this study.

Instead of the above mentioned large deformation numerical analysis, small deformation numerical analysis is used to simulate the progressive spudcan penetration. This present study employs Press-Replace (PR) Technique, which based on a small-strain geometry update procedure. This technique has been successfully used to handle the large deformations problem and incorporate the installation effects around a wished-in-place pile. Furthermore, PR Technique can be applied in standard finite element packages commonly used in geotechnical practice.

1.2 Thesis objective

The main objective of the present study is:
'To investigate the load penetration curve of spudcan foundations of offshore jack-up rigs based on wished-in-place footing'

Axisymmetric finite element analysis, using PLAXIS 2D, is used to analyze the penetration process of spudcan foundations subjected to vertical loading.
The following sub-objectives might be considered:

- To exploit PR (Press-Replace) Technique for spudcan penetration process.
- To produce spudcan penetration curves for different soil profiles, soil properties and spudcan foundation geometries.
- To produce normalized design charts.
- To further understand the spudcan penetration process in layered soils.

The current research only investigates the spudcan penetration in two soil types, namely sand (drained analysis) and clay (undrained analysis) with Mohr Coulomb as the constitutive soil model. The study includes penetration in two layer systems, while three layered soil or more is considered outside the scope of the current study. Soil configurations that have been explored are:

- Single layer clay with homogeneous and nonhomogeneous strength profiles.
- Single layer sand (loose and medium dense sand).
- Loose sand over clay with increasing strength profiles.

Moreover, this study only focuses on the performance of spudcan under vertical loading condition. Thus, other site-specific assessments mentioned below are not considered in the current research:

- Yield interaction check, which is the limiting combinations of the spudcan moment, vertical and horizontal reactions.
- Sliding check.

1.3 Thesis outline

This research consists of roughly three parts: literature review, development of the numerical model, and parametric study.

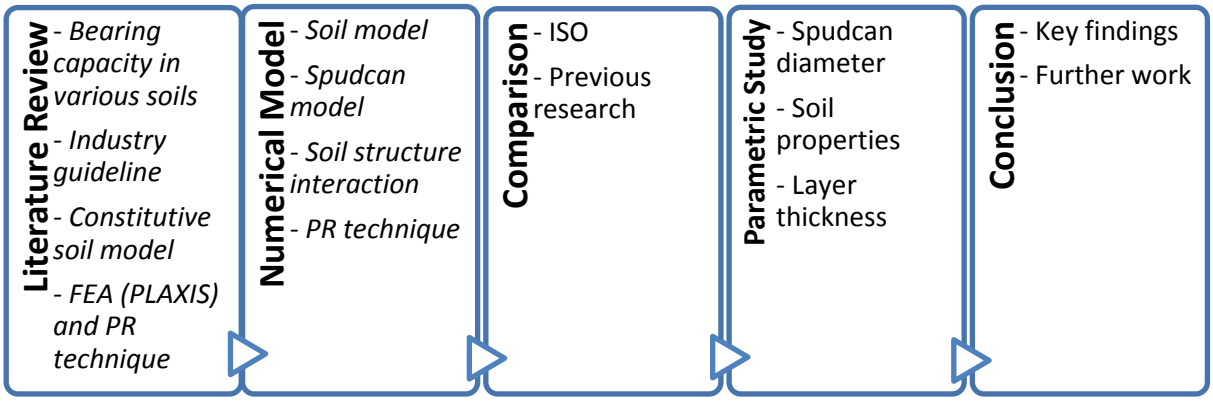

Figure 1-4 Outline

Firstly, Chapter 2 provides literature review related to the bearing capacity of vertically loaded foundation on sand, clay, and sand over clay. The existing experimental and numerical findings are also included in this chapter.

Chapter 3 describes the numerical model framework of spudcan penetration. This chapter not only gives the introduction of the finite element package, PLAXIS 2D 2015, but also the constitutive soil model used in this research. The PR (Press-Replace) Technique introduced by Engin (2013) is employed to simulate the spudcan penetration process and the method is also explained in this chapter.

The finite element analyses start with the single layer system, penetration in sand and in clay (Chapter 4). Chapter 5 presents the results of finite element analyses which are conducted for double layered system. A parametric study is also carried out in each chapter.

Chapter 6 summarizes the main findings of this study and gives recommendation for future research.

Chapter 2.
Background on Spudcan Penetration

This chapter provides a brief overview of methods for calculating the bearing capacity of vertically loaded foundations in different soil conditions. Inclined and horizontal loads are excluded. The discussion focuses on the classical bearing capacity approach, the current design guideline in ISO 19905-1: 2012, and findings from previous research. Two soil types, clay and silica sand, are presented. Other soil types are neglected in this study although they might be encountered offshore.

2.1 General concept

The penetration assessment of spudcan foundation is commonly predicted by considering the bearing capacity of a series of "wished-in-place" footing at different depths and the resistance profiles are generally assessed within the framework used for onshore application. Following Prandtl (1921), Terzaghi (1943) extended the conventional bearing capacity theory which is based on plasticity theory. It is assumed that the soil is rigid-perfectly plastic with the strength denoted by a cohesion (c), a friction angle (φ), and an effective unit weight (γ'). Assuming the separate contributions of the strength parameters, Terzaghi's bearing capacity equation can be conveniently expressed as:

$$q_u = c\,N_c + q\,N_q + 0.5\,\gamma\,B\,N_\gamma \tag{2-1}$$

$$N_c = \left(N_q - 1\right)\cot\varphi \tag{2-2}$$

$$N_q = exp^{\pi\tan(\varphi)}tan^2(45^o + \frac{\varphi}{2}) \tag{2-3}$$

$$N_\gamma = 1.5\left(N_q - 1\right)\tan\varphi \tag{2-4}$$

The terms N_c, N_q, and N_γ are the bearing capacity factors which are respectively, the contributions of cohesion, surcharge, and unit weight of the soil to the ultimate bearing capacity (q_u). N_c and N_q are expressed as a function of friction angle, φ. For the limiting case however, when φ= 0, the value of N_c is equal to 5.142 ($N_c \approx \pi + 2$). Hence, only N_c and N_q are applicable for calculating bearing capacity in clay (undrained condition, where φ is set to zero) since N_γ equals zero. On the other hand, for cohesionless soil (c= 0) such as sand, the N_q and N_γ are relevant to calculate the bearing capacity.

Bearing capacity factors are originally developed for strip footings. Equation 2-2 and 2-3 are proposed by Meyerhof (1963) to calculate N_c and N_q. Unlike N_c and N_q, several suggestions have been made to calculate N_γ, for example the expression in equation 2-4 which is proposed by Hansen (1970). Other authors such as Vesic (1975) and Meyerhof (1963) also proposed solutions with slightly different expressions. It should be noted that this traditional formula can be extended to cope with different shapes of the loaded footing, the inclination of the load and embedded foundations. Figure 2-1 shows conventional failure mechanism based on Prandtl (1921) which uses a subdivision of the soil intro three zones.

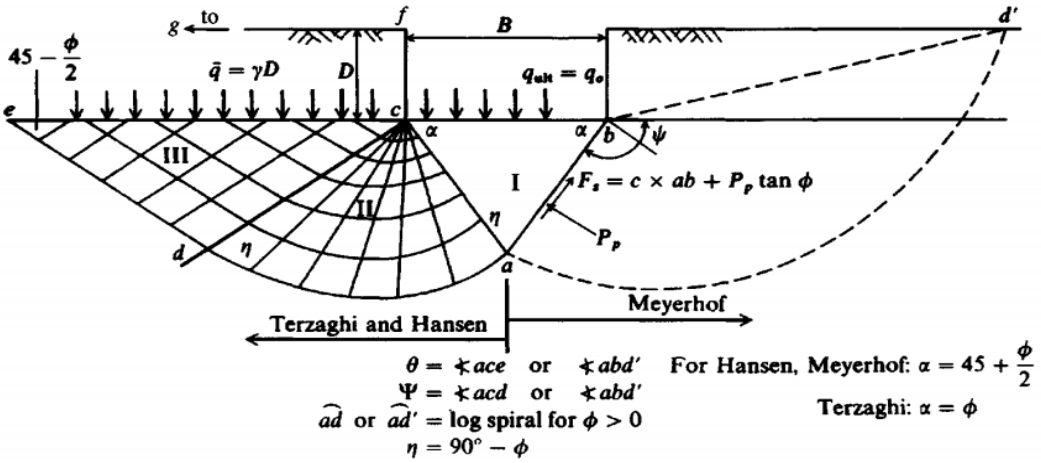

Figure 2-1 General footing-soil interaction for bearing capacity equations for strip footing (Bowles, 1997).

This failure mechanism will be derived here. Generally, when the foundation is loaded, Zone I (elastic zone, in which the vertical normal stress is equal to the load on top of the foundation) is pushed down, and it presses Zone II (radial shear zones) and III (passive zone, where the horizontal stress is larger than the vertical stress which is equal to the surcharge load, q) sideways and then upward. Figure 2-1 also qualitatively shows the slip lines that illustrate stress trajectories in the plastic zone beneath the foundation (Bowles, 1997).

2.2 Bearing capacity in sand

Drained bearing capacity calculation, in which no excess pore water pressure is generated, is normally used to evaluate the spudcan penetration in silica sand. The spudcan is often modelled as a flat circular foundation for conventional foundation analyses. One of the most commonly used methods is the method proposed by Hansen (1970) which is also recommended by ISO 19905:1-2012. Embedment depth factors (d_q and d_γ) are introduced to incorporate the shearing resistance developed by overlying soil above the base of the foundation.

$$Q_v = \frac{\gamma' d_\gamma N_\gamma \pi B^3}{8} + \frac{p'_o d_q N_q \pi B^2}{4} \tag{2-5}$$

$$d_q = 1 + 2\tan\varphi'(1-\sin\varphi')^2 \, tan^{-1}\left(\frac{d}{B}\right) \tag{2-6}$$

$$d_\gamma = 1 \text{ ; (for drained soil)}$$

$$N_q = exp^{\pi \tan(\varphi)} tan^2(45^o + \frac{\varphi}{2}) \tag{2-7}$$

$$N_\gamma = 1.5\left(N_q - 1\right)\tan\varphi \tag{2-8}$$

ISO 19905-1: 2012 also provides theoretical values of N_q and N_γ, calculated with the slip-line method implemented into the ABC program by Martin (2003). The values are valid for a flat, rough circular footing and for friction angle from 20° to 40°. Furthermore, more detailed analyses using the values of N_γ that take into account conical shape of the footing and interface roughness coefficients (α) are also given in the Annex of ISO 19905-1:2012. The theoretical values of N_γ were calculated by Cassidy

and Houlsby (2002) and could be applied to any conical footing on sand that cover cone apex angles (β) from 60° to 180°.

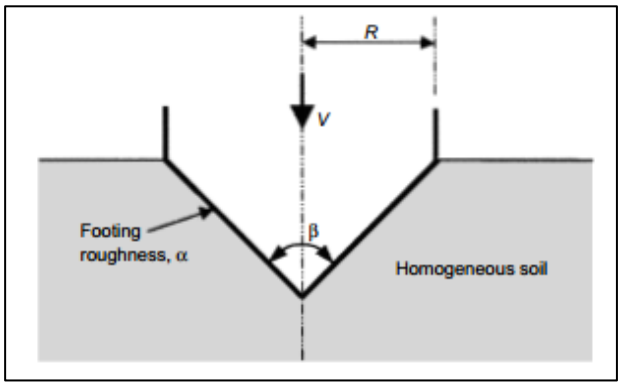

Figure 2-2 Problem definition and notation used by Cassidy and Houlsby (2002).

It should be highlighted that the bearing capacity calculated using equation by ISO 19905-1: 2012 is highly dependent on the soil friction angle, φ. Therefore, the value of φ should be carefully chosen. White et al. (2008) emphasized that the key uncertainty in the prediction of spudcan bearing capacity is the assessment of an appropriate friction angle. White et al. (2008) further reported that the difference in N_γ is because of the reduction in operative friction angle due to progressive failure rather than attributed to footing roughness and conical geometry. Another industry guideline, SNAME 2008, recommends to have a reduction of 5° of friction angle obtained by triaxial laboratory tests while The InSafeJIP Guideline prefers to use the value from laboratory and then apply the reduction factor.

One can also calculate the vertical load capacity with the equation derived by Cassidy and Houlsby (1999) which combines theoretical and experimental ideas and implements a work hardening plasticity model for spudcan footings on dense sand. New constant factor, s_{fp}, is introduced in this approach.

$$V_o = s_{fp}\gamma N_\gamma \pi \left(w_p \tan\left(\frac{\beta}{2}\right)\right)^3 \tag{2-9}$$

$$s_{fp} = \frac{\frac{k\,w_p}{V_{Om}} + \left(\frac{f}{1-f_p}\right)\left(\frac{w_p}{R\,\delta}\right)^2}{1 + \left(\frac{k\,w_p}{V_{Om}} - 2\right)\frac{w}{R\delta_p} + \left(\frac{1}{1-f_p}\right)\left(\frac{w}{R\delta_p}\right)^2} \tag{2-10}$$

$$f = 0.1\ and\ \delta_p = 0.3\ (from\ experiment)$$

where k is the initial plastic stiffness, w the vertical displacement, w_p the plastic vertical displacement, f_p the dimensionless constant that describes the limiting magnitude of vertical load of V_{0m}, and δ is the dissipation parameter. Moreover, It is suggested to use bearing capacity factor, N_γ, value from Bolton and Lau (1993).

For penetration on a uniform sand layer, the phenomena called backflow and infill are rarely possible (ISO 19905-1, 2012). Soil backflow is initiated at a certain penetration depth. It limits the

cavity depth and provides seal on top of the spudcan. Infill, in addition, is caused by soil coming from the sediment transport or the collapsing sidewall. Backflow might be feasible in loose sands, however, or infill might be feasible when spudcan is placed in the sites where moving sandbanks occur. The difference between backflow and infill is depicted in Figure 2-3.

Key

1. Backflow
2. Infill – wall failure
3. Infill – sediment transport
4. Region subject to infill processes
5. Region subject to backflow

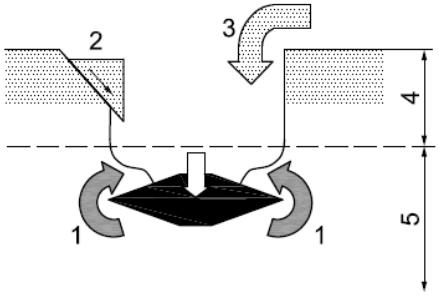

Figure 2-3 Backflow and infill (ISO 19905-1, 2012).

2.3 Bearing capacity in clay

Most industry guidelines agree on the method for calculating spudcan penetration in clay, with a homogeneous shear strength distribution, by an idealized flat circular foundation of diameter, *B*, embedded at depth, *d*, below the seabed level, using bearing capacity factor formulations proposed by Skempton (1951).

$$Q_v = (s_u N_c s_c d_c + p'_o)A \tag{2-11}$$

$$d_c = 1 + 0.2\,\frac{d}{B} \leq 1.5 \tag{2-12}$$

$N_c s_c = 6.0$; for circular footings.

p'_o is the effective overburden pressure at depth, *d*.

In order to select the design undrained shear strength, ISO 19905-1: 2012 notes that: "an evaluation should be made of the sampling method, the laboratory test type and the field experience regarding the prediction and observations of spudcan penetrations."; also "for typical Gulf of Mexico shear strength gradients and spudcan dimensions, spudcan penetrations in clay are well predicted by selecting s_u as the average over a depth of $B/2$ below the widest cross-section."

As an alternative for bearing capacity factor (N_c), solutions provided by Houlsby and Martin (2003) can be used which gives theoretical lower bound to the soil resistance. The proposed algebraic expressions can be exploited for shallow circular foundations, accounting for embedment (*d*), cone angle (β), rate of increase of strength with depth (*k*), and surface roughness of the foundation (α).

$$N_c = N_{c0\alpha} + \frac{\alpha}{\tan\left(\frac{\beta}{2}\right)}\left[1 + \frac{1}{6\tan\left(\frac{\beta}{2}\right)}\frac{Bk}{s_{u0}}\right] \tag{2-13}$$

$$N_{c0\alpha} = N_{c00}\left[1 + (0.212\alpha - 0.097\alpha^2)(1 - 0.53\frac{d}{B+d})\right] \tag{2-14}$$

$$N_{c00} = N_1 + N_2 \frac{Bk}{S_{u0}} \tag{2-15}$$

$$N_1 = 5.69 + \left[1 - 0.21 \cos\left(\frac{\beta}{2}\right)\right]\left(1 + \frac{d}{B}\right)^{0.34} \tag{2-16}$$

$$N_2 = 0.5 + 0.36 \left[\frac{1}{tan\left(\frac{\beta}{2}\right)}\right]^{1.5} - 0.4\left(\frac{d}{B}\right)^2 \tag{2-17}$$

In all analyses the soil was assumed to be weightless and the cavity above the conical footing is assumed to be occupied by a rigid but smooth-sided cylindrical shaft. The N_c values proposed by Houlsby and Martin (2003) are also tabulated and presented in the Annex E1 of ISO 19905-1: 2012.

Unlike the study by Houlsby and Martin (2003), more recent study by Salgado et al. (2004) did not ignore the soil weight, so that the proposed bearing capacity factors can be more applicable for a spudcan foundation where soil can freely flow back on top of the spudcan. Salgado et al. (2004) reported the bearing capacity factors in uniform clay (kB/s_{um}= 0) based on finite element limit analysis. Lower and upper bound values were proposed for rough strip, circular, square, and rectangular foundations. Table 2-1 shows the result by Salgado et al. (2004) for circular footing.

Table 2-1 Bearing capacity factors, s_c N_c d_c, for circular footing in clay (Salgado et al., 2004).

d/B	Lower Bound	Upper Bound
0	5.856	6.227
0.01	5.164	6.503
0.05	5.293	6.840
0.10	5.448	7.140
0.20	5.696	7.523
0.40	6.029	8.104
0.60	6.240	8.608
0.80	6.411	9.034
1.00	6.562	9.429
2.00	7.130	11.008
3.00	7.547	12.140
4.00	7.885	13.030
5.00	8.168	13.743

Moreover, Hossain et al. (2006) used both centrifuge model tests and large deformation finite element analysis (LDFE) to propose new mechanism design approach for spudcan foundation on single layer clay with uniform strength and nonhomogeneous clay, with *k* as a gradient of the undrained shear strength which is linear with depth. The results from experimental results exhibit similar trends to those from the LDFE analyses. Hossain and Randolph (2009) proposed the following formula to compute bearing capacity factors:

- *Homogeneous clay*

$$N_{cd} = 5.69 + \frac{d}{0.22H}\left(1 - \frac{d}{5.8H}\right) \leq 12 \quad smooth\ base \tag{2-18}$$

$$N_{cd} = 6.05 + \frac{d}{0.21H}\left(1 - \frac{d}{6.2H}\right) \leq 13.1 \quad rough\ base \tag{2-19}$$

- *Nonhomogeneous clay*

$$N_{c0k} = N_{c0}\left[1 + \frac{0.161\left(\frac{kd}{s_{u0}}\right)^{0.8}}{\left(1 + \frac{d}{B}\right)^{2}}\right] \quad smooth\ base \tag{2-20}$$

$$N_{c0k} = N_{c0}\left[1 + \frac{0.191\left(\frac{kd}{s_{u0}}\right)^{0.8}}{\left(1 + \frac{d}{B}\right)^{1.5}}\right] \quad rough\ base \tag{2-21}$$

To take into account the increase of soil strength over the depth, equations 2-20 and 2-21 are introduced, which also adjust the N_{c0}-values of uniform clay. Table 2-2 gives N_{c0}-values for calculating bearing capacity factors of non-homogeneous clay.

Table 2-2 N_{c0} values for spudcan penetration on uniform clay.

d/B	N_{c0}	
	smooth	Rough
0	5.45	6.07
0.083	6.2	6.85
0.167	6.64	7.21
0.25	7	7.48
0.333	7.29	7.75
0.417	7.57	798
0.5	7.8	8.19
0.583	8.03	8.41
0.75	8.46	8.76
0.833	8.66	8.95
1	8.95	9.25
1.25	9.2	9.7
1.5	9.2	10.1
2	9.2	10.15
2.5	9.2	10.15
3	9.2	10.15

Hossain (2008) also underlined three distinct mechanisms of soil flow around the advancing spudcan: (a) outward and upward flow leading to surface heave and formation of a cavity above the spudcan; (b) gradual flow back into the cavity; and (c) fully localized flow around the embedded spudcan with the unchanging cavity. At a certain stage of penetration, soil backflow is initiated, which provides a seal above the spudcan and limits the cavity depth (*H*). ISO 19905-1: 2012 gives the following equation to calculate cavity depth, based on the experiments by Hossain (2008):

- *Uniform shear strength*

$$\frac{H_{cav}}{B} = S^{0.55} - \frac{S}{4} \tag{2-22}$$

$$S = \left(\frac{s_{um}}{\gamma' B}\right)^{\left(1-\frac{\rho}{\gamma'}\right)} \tag{2-23}$$

- *Multi-layer clays with moderate changes of strength*

$$\frac{H_{cav}}{B} = \left(\frac{s_{uH}}{\gamma' B}\right)^{0.55} - \frac{1}{4}\left(\frac{s_{uH}}{\gamma' B}\right) \tag{2-24}$$

The subsequent backflow continues below the limiting cavity depth and above the advancing spudcan, i.e. the initial cavity is not filled up by the backflow process – see Figure 2-4(c).

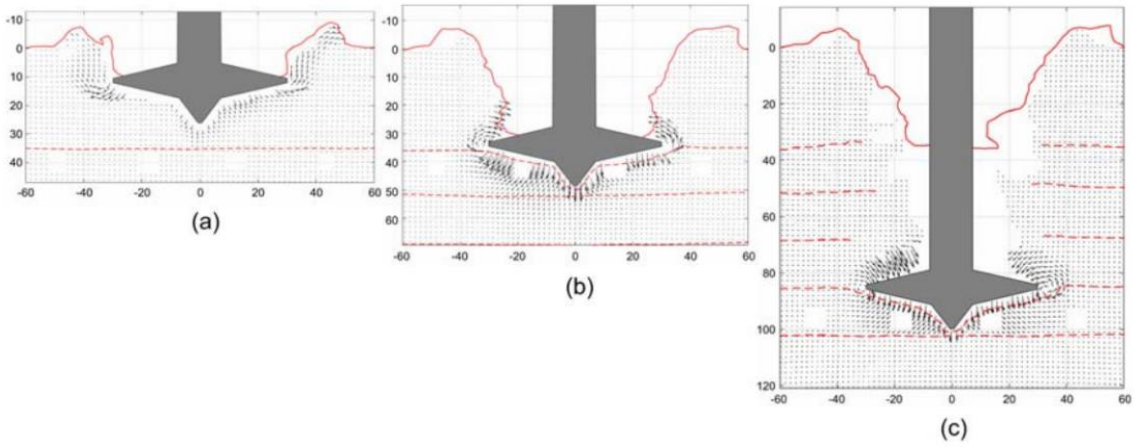

Figure 2-4 Flow mechanism for spudcan penetration on clay (Hossain & Randolph, 2009).

Where s_{uH} is the shear strength at the backflow depth, H_{cav}. Iteration is needed to establish the consistent values of H_{cav}/B and s_{uH}. Equations 2-22 and 2-23 are graphically presented in Figure 2-5.

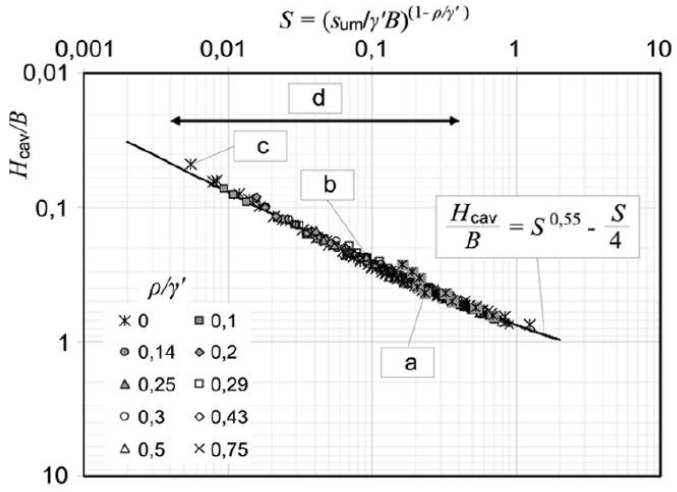

Figure 2-5 Estimation of limiting cavity depth, H_{cav} ("ISO 19905-1," 2012)

2.4 Bearing capacity in sand over clay

Layered soil deposits are commonly encountered in practice. A potential installation problem, known as punch-through, might be triggered as spudcan penetrates into strong overlying soft soils, for instance in spudcan penetrating into sand-over-clay or stiff clay-over-soft clay. Figure 2-6 shows the illustration of load penetration curve with a punch-through failure. The resistance increases until the peak resistance (q_{peak}) is achieved and then followed by the reduction of the penetration resistance. The unexpected punch-through failure might lead to buckling of the leg or even toppling of the jack-up unit.

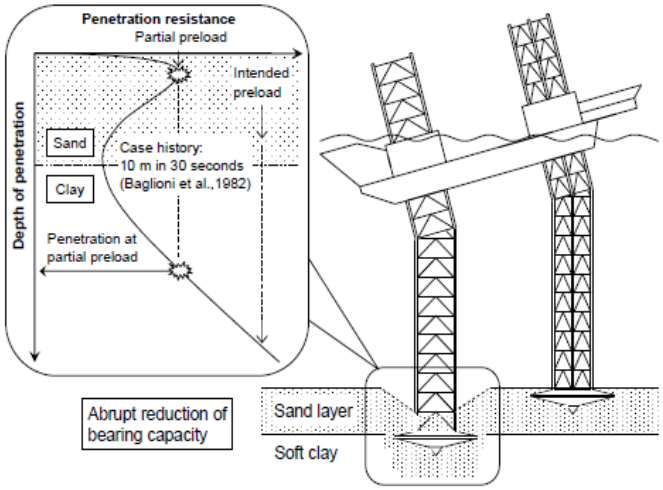

Figure 2-6 Illustration of punch-through failure during pre-load(Lee, 2009).

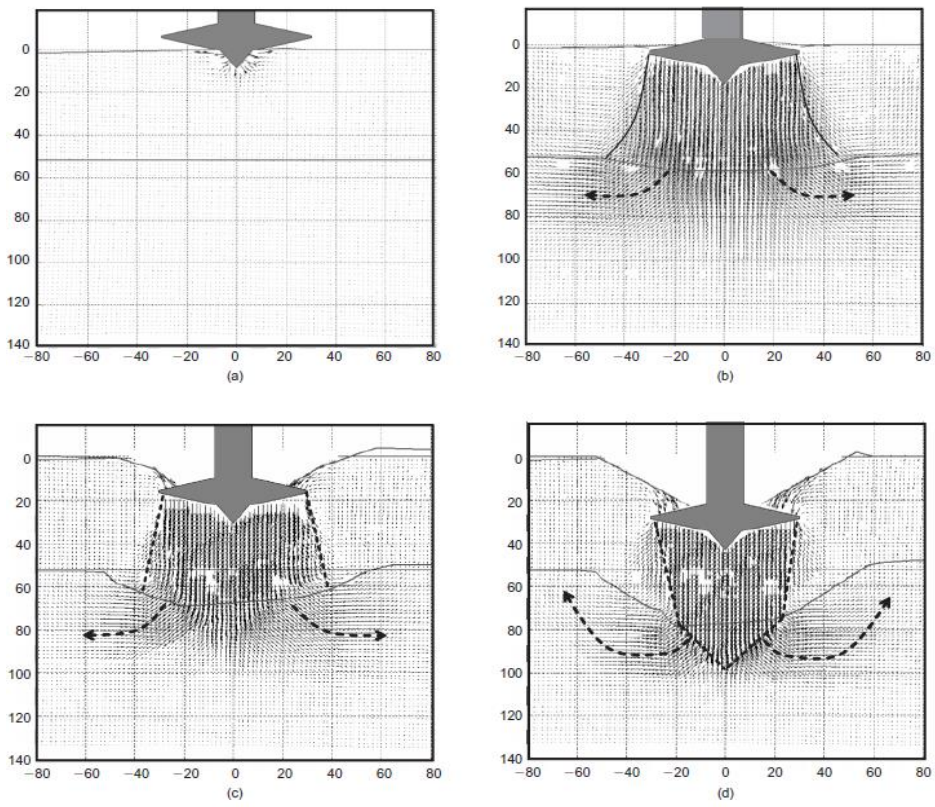

Figure 2-7 Spudcan failure mechanism at different penetration depths (Teh et al., 2008).

Figure 2-7 shows failure mechanism at different penetration depths as spudcan penetrates through sand overlying clay. At a certain depth (relatively shallow penetration depth), the failure mechanism extends to the clay deposit, which is less strong than the upper sand layer – see Figure 2-7(b). The reduction on the penetration resistance is because of this strength contrast between the upper and lower layer.

The ISO 19905-1:2012 recommends two methods to calculate peak resistance of spudcan on sand overlying clay, namely load spread model and punching shear mechanism.

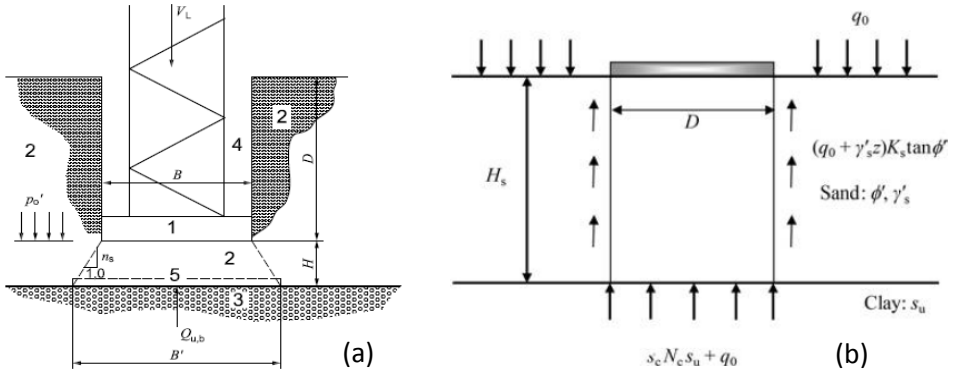

Figure 2-8 (a) Load spread method (ISO 19905-1, 2012). (b) Punching shear method of ISO 2012 (Cassidy et al., 2015).

As illustrated in Figure 2-8(a), load spread method considers a fictitious footing (5) at the interface between the sand (2) and clay (3) layers. This method uses load spread factor, n_s, which is in the range of 3 to 5 (ISO 19905-1, 2012), to calculate the bearing capacity of fictitious spudcan. The peak capacity can then be obtained by subtracting the weight of the sand (W) between the spudcan and fictitious footing from the fictitious footing's capacity ($Q_{u,b}$).

$$W = 0.25\,\pi \left(B + 2\frac{H_s}{n_s}\right)^2 H\,\gamma' \tag{2-25}$$

$$Q_v = Q_{u,b} - W \tag{2-26}$$

$Q_{u,b}$ can be calculated using equation 2-11 in the previous section.

The latter approach, punching shear mechanism, is originally developed by Hanna and Meyerhof (1980) for shallow wished-in-place footings. Vertical shear plane is used to calculate the peak resistance as illustrated in Figure 2-8(b) and can be expressed as:

$$q_{peak} = N_c s_u + \frac{2H_s}{D}\left(\gamma'_s H_s + 2q_o\right) K_s tan\phi' + q_o \tag{2-27}$$

where D in the expression above is equal to the effective maximum diameter of the spudcan, B. New coefficient, K_s, is introduced to account for the frictional resistance on the assumed vertical plane. ISO 19905-1:2012 also provides graph, see section A.9.3.2.6.4 of the guideline, to calculate K_s that depends on the strength of both the sand layer and the clay layer. Beyond the sand-clay interface, ISO 19905-1:2012 recommends to assess the resistance as a foundation in a single layer clay.

However, Lee et al. (2013) and Hu et al. (2014) showed that both methods underestimate the potential of punch-through. Hence, several research has been undertaken to improve the understanding of the spudcan penetration in sand overlying clay that generally has two prominent phases: (i) peak resistance in the sand layer, and (ii) resistance in the underlying clay layer.

Figure 2-9 presents nomenclature for spudcan foundation penetration in sand overlying clay. It should be noted that *B* is used instead of *D* to indicate spudcan diameter in the present study.

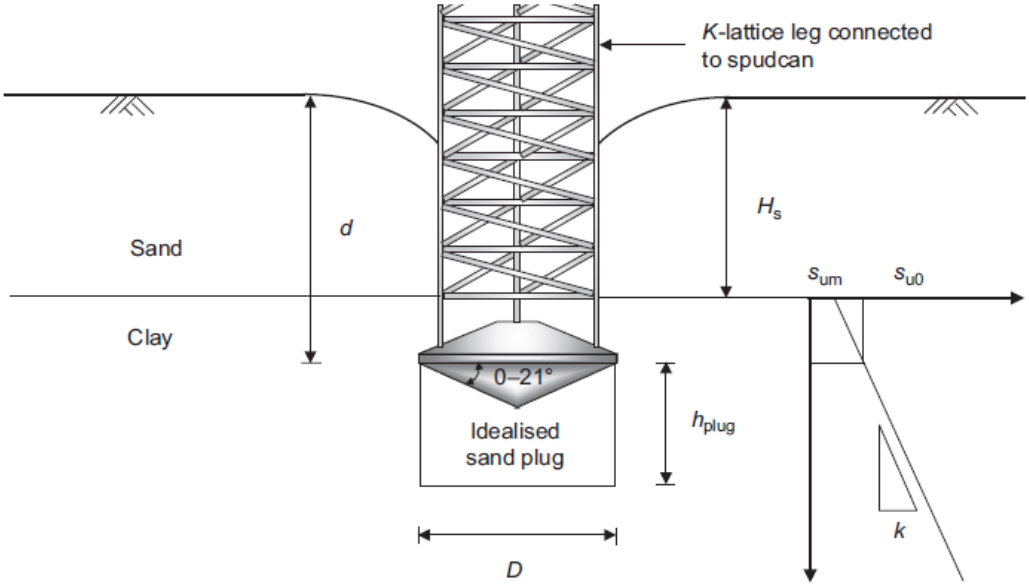

Figure 2-9 Schematic diagram of spudcan foundation penetration in sand overlying clay (Hu et al., 2015).

Teh (2007) used particle image velocimetry (PIV) analysis and centrifuge test to study spudcan bearing capacity in dense sand overlying clay and proposed a design framework to estimate the peak resistance, q_{peak}. Based on the observations of Teh (2007), Lee (2009) also proposed a new conceptual model to calculate q_{peak} using drum centrifuge test and FE analyses. The method takes into account the stress-level and dilatant response of the sand layer. Then, this model was extended by Hu et al. (2014) to account for mobilization depth. Most recently, Bienen et al. (2015) established the-state-of-the-art in understanding of spudcan penetration into sand overlying clay based on cone penetration (CPT) resistance. It was also observed in all literatures that the peak resistance occurs at a relative shallow embedment, ≈ $0.12H_s$ – $0.18H_s$, where H_s is the sand layer thickness.

According to observations from experiments and finite element analysis by Teh (2007), Lee (2009), and Hu et al. (2014), calculating the bearing capacity becomes more complicated due to the uncertainty of the sand trapped underneath the spudcan once it penetrates into the clay layer. The shape and thickness of the sand trapped underneath the spudcan might change as some sand escapes and flows around the foundation during the penetration process (Lee, 2009). It should be noted that both methods in ISO guideline ignore the contribution of the sand plug. The maximum sand plug height can be approximated as $0.9H_s$ based on the testing and numerical data by Hu et al. (2014). Hu et al. (2014) further reported that the bearing capacity of a spudcan in clay can be expressed as:

$$q_{clay} = N_{c,pp}\, s_{uo} + H_{plug}\gamma'_c \qquad (2\text{-}28)$$

Besides the study of punch-through failure of spudcan on dense or very dense overlying clay by Teh (2007), Lee (2009), and Hu et al. (2014), Yu et al. (2012) investigated the spudcan penetration in loose sand overlying clay using the large deformation analysis and showed that the current industry guideline underestimates the peak bearing capacity of the spudcan compared to the numerical results.

Several equations below show the expressions of post peak bearing capacity factors ($N_{c,pp}$) found in literatures for spudcan penetrating the underlying clay layer.

$$N_{c,pp} = 3.3\left(\frac{H_s \gamma'_s \tan\varphi'}{s_{uo}}\right) + 9{,}5 \quad ; \left(0{,}21 \le \frac{H_s}{B} \le 1.12\right); \text{ proposed by Yu et al. (2012)} \tag{2-29}$$

$$N_{c,pp} = 14\frac{H_s}{B} + 9{,}5 \; ; \left(0{,}21 \le \frac{H_s}{B} \le 1.12\right); \text{ proposed by Lee et al. (2013)} \tag{2-30}$$

$$N_{c,pp} = 15\frac{H_s}{B} + 9 \quad ; \left(0{,}16 \le \frac{H_s}{B} \le 1\right); \text{ proposed by Hu et al. (2014)} \tag{2-31}$$

2.5 Conclusion

Several methods to calculate bearing capacity of vertically loaded spudcan have been briefly presented in this chapter. It is apparent that issues related to spudcan penetration still attract many researchers to get a better understanding of the penetration process, especially for layered system. Although a conventional approach is still commonly used in the industry guidelines, it is evident that researchers tend to conduct experiments or numerical analyses to investigate this problem.

The methods described in this chapter are used as a benchmark for verifying the proposed alternative method to assess spudcan bearing capacity profile for penetration in sand, clay, and sand overlying clay in this study.

Chapter 3.
Numerical Model

The penetration depth of spudcan foundation is normally predicted by considering “wished-in-place” approach following traditional bearing capacity solutions although in reality spudcan penetration is a continuous process. Analysis based on numerical modelling is one possible option to evaluate spudcan penetration depth. In order to correctly simulate this continuous process, especially in multiple layer systems, large deformation analysis method is required. However, it is beyond the scope of the current study. Instead, a small deformation analysis is used with a simple soil constitutive model, following the approach commonly used by the industry, “wished-in-place” footing. This chapter gives a short introduction to the commercial finite element package used in this study, the chosen constitutive soil model, and also the technique employed to simulate the spudcan installation during preloading.

3.1 Introduction to PLAXIS

All the FE analyses in this study are performed using the commercial finite element software, PLAXIS, which is specially developed to perform deformation and stability analysis for various types of geotechnical applications. PLAXIS 2D 2015 is used for all numerical simulations.

3.1.1 General

The FE analyses are carried out using a two dimensional axisymmetric model. A 2D axisymmetric model can be chosen since spudcan foundation can be represented as a circular structures with an uniform radial cross section and it is only vertically loaded during the preloading, horizontal loading is neglected in this stage.

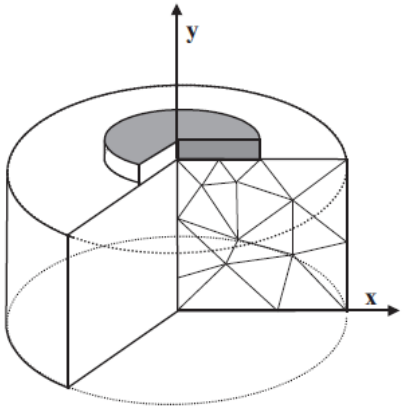

Figure 3-1 Illustration of axisymmetric model (Brinkgreve et al., 2015).

Two types of element are available in PLAXIS to model soil layers and other volume clusters, 15-node triangle and 6-node triangle. In addition, it is recommended to use the 15-node triangle elements when axisymmetric model is chosen since these elements are more accurate, compared to 6-node elements, to model a situation where failure plays a role, for example in a bearing capacity calculation (Brinkgreve et al., 2015). The 15 node triangle elements provide high quality stress results in this case.

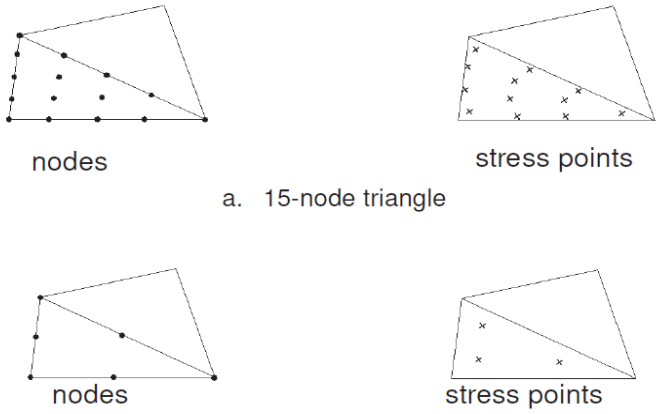

Figure 3-2 Position of nodes and stress points in soil elements (Brinkgreve et al., 2015).

3.1.2 Boundary conditions and mesh size

Foundations, in general, are very stiff compared to the soil and are often analysed using two extreme assumptions, namely flexible foundation or rigid foundation. Once the foundation is assumed as a rigid foundation, all the analyses can be performed under load or displacement control method (Potts & Zdravkovic, 1999). Figure 3-3 shows various alternatives for the boundary conditions to be applied below the footing. ΔF_y is the applied load, ΔF_x the horizontal nodal forces, Δ_u the horizontal displacement, and Δ_v is the vertical displacement. In the current study, the spudcan is modelled as a rigid foundation by applying prescribed vertical displacements. Then, the footing load can be obtained by summing all the vertical reactions of the nodes which have been subjected to this displacement.

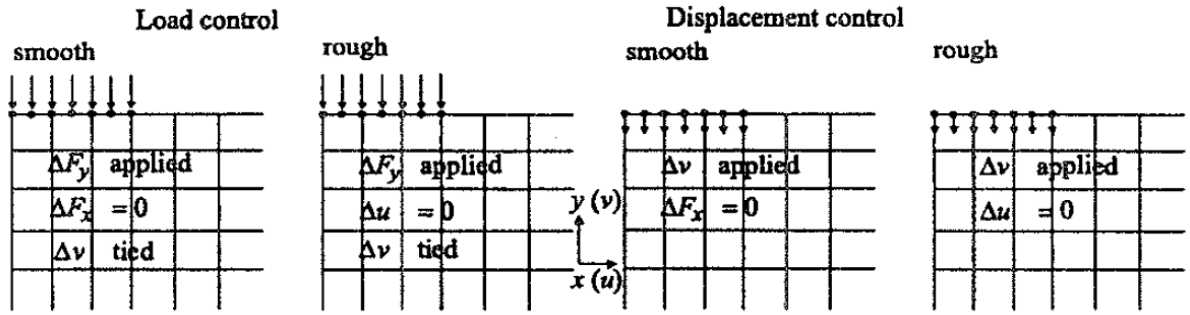

Figure 3-3 Options for rigid footing (Potts & Zdravkovic, 1999).

Furthermore, lateral and bottom boundary distance (L_{BD} & B_{BD}) are initially set at ten foundation diameters from the centre of the foundation and the surface – see Figure 3-4. This condition is found to be suitable as a reference case without the effect of the boundary distance on penetration response (Ullah et al., 2014). The effect of the boundary condition will be investigated when the L_{BD} & B_{BD} size are reduced and presented in the next chapter.

Interface element should also be defined in order to model a proper interaction between spudcan and soil. The choice of soil-structure interaction for numerical modelling might have significant influence on the outcomes. One possible option to define the interface in PLAXIS is using a reduction factor ($R_{inter} \leq 1.0$) applied to the soil material when defining soil property values (the default value is

R_{inter}= 1.0, i.e. a fully-bonded interface). Hence, the interface strength (wall friction and adhesion) relates to the shear strength (friction angle and cohesion) of the adjacent soil. Interface property value will parametrically be studied in the next chapter. The following equations show how interface properties are calculated in PLAXIS.

$$c_i = R_{inter}\, c_{soil} \tag{3-1}$$

$$tan\, \phi_i = R_{inter}\, tan\, \phi_{soil} \tag{3-2}$$

$$G_i = R_{inter}^2\, G_{soil} \tag{3-3}$$

$$E_i = 2\, G_i\, (1 + \nu_i) \tag{3-4}$$

$$\nu_i = 0.45 \tag{3-5}$$

$$E_{oed,i} = 2\, G_i\, \frac{1 - \nu_i}{1 - 2\nu_i} \tag{3-6}$$

In the case of extended interfaces, the strength of these interfaces should be assigned as Rigid (R_{inter} = 1) since those are not intended for soil-structure interaction and should not have reduced strength properties. Extended interface is an additional interface element inside the soil body that will solve poor quality stress results around the corner point of a structure (Brinkgreve et al., 2015).

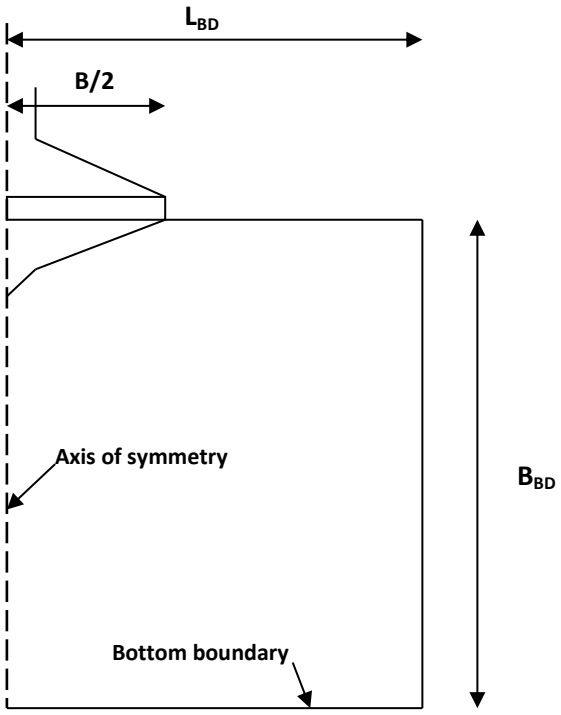

Figure 3-4 Illustration of boundary effect problem.

In PLAXIS, mesh size can be automatically generated in the *Mesh Mode* which discretize the geometry model and transform to a finite element mesh. In this research, the effect of mesh density will be little looked over by following the recommendation from the study of the dependency of the solution on the mesh size by Engin (2013).

3.2 Constitutive soil model

Mohr-Coulomb Model is chosen in this study. It is a well-known linear elastic perfectly plastic model that is based on Hooke's law of isotropic elasticity (linear elastic) and Mohr-Coulomb failure criterion (perfectly plastic). The basic principle of any elastic-plastic model is that strain increments can be divided into elastic (recoverable) and plastic (irrecoverable) parts:

$$\{\delta\varepsilon\} = \{\delta\varepsilon^e\} + \{\delta\,\varepsilon^p\} \tag{3-7}$$

Figure 3-5 shows the idealized behaviour of a material conforming elastic-perfectly plastic model. It can be seen that plasticity is equal to failure in this model.

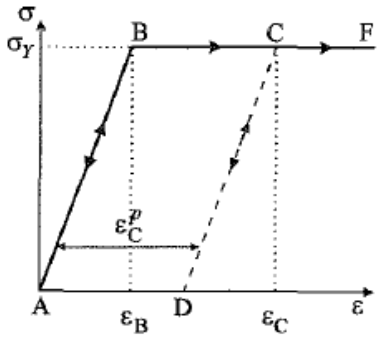

Figure 3-5 Elastic-perfectly plastic model (Potts & Zdravkovic, 1999).

Failure criteria needs to be included in the elastic model to define the stress states which cause plastic deformations. Plastic yielding takes place when the yield function is above zero. Mohr Coulomb failure criterion is adopted as the yield function. An example of a yield criterion is expressed, as follow:

$$f = {}^1\!/_2\,(\sigma'_1 - \sigma'_3) - c\,cos\,\varphi' + {}^1\!/_2\,(\sigma'_1 + \sigma'_3)\,sin\varphi' \tag{3-8}$$

σ'_1 and σ'_3 are the principal effective stresses, major and minor respectively. The yield function resolves into an irregular hexagonal pyramid once mapped into 3D stress space as shown in the Figure 3-6.

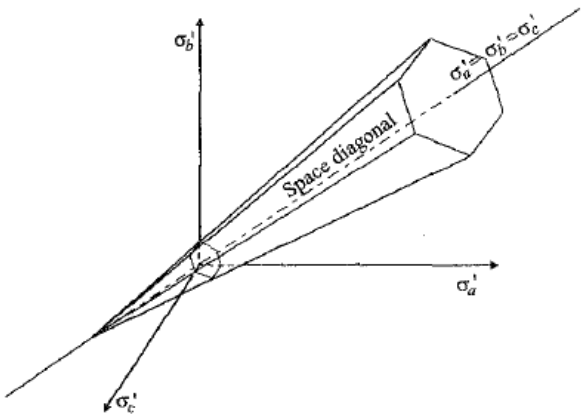

Figure 3-6 Mohr Coulomb failure surface (Potts & Zdravkovic, 1999).

In addition to the yield function, a plastic potential function is required to describe plastic strains and similar form to that yield function is used but with φ' replaced by ψ in order to accurately represent dilatancy. See example below for the plastic potential function expression.

$$g = {}^{1}/_{2}\,(\sigma'_1 - \sigma'_3) - c\cos\psi + {}^{1}/_{2}\,(\sigma'_1 + \sigma'_3)\sin\psi \tag{3-9}$$

It should be emphasized that no hardening or softening law is required, as the Mohr-Coulomb model is assumed to be perfectly plastic. Wood (2004) stated a drawback using this model, which can only describe the final failure condition together with either initial stiffness or some average stiffness of a stress state intermediate between the beginning and end of test. This will not give an accurate description of the behaviour at any soil element.

Despite the downside, it is well-known that Mohr-Coulomb model is widely used because of their simplicity and capability as a first approximation of soil behaviour. Several investigators have implemented Mohr-Coulomb failure criterion and found it to be sufficiently accurate for most geotechnical applications (Chen & Saleeb, 1983). In order to use the Mohr-Coulomb model, 5 parameters are required. Three of these, *c,* φ, and ψ, control the plastic behaviour, and the remaining two, *E* and *v*, control the elastic behaviour.

3.3 Undrained and drained analysis

In the present study, the soil is assumed to be either fully undrained or drained. The clay is assumed to be fully undrained in all analyses, in which the stiffness matrix is expressed in terms of total stress parameters, and based on an undrained Young modulus and an undrained Poisson's ratio (Wood, 2004).

Furthermore, the drainage type *Undrained (C)* is used in PLAXIS. Volumetric change is not allowed using this drainage type and undrained shear strength, s_u, is an input for the model. Poisson's ratio value of 0.495 is normally applied for undrained analysis, although ideally Poisson's ratio equal to 0,5 is set for an isotropic elastic soil. Setting the Poisson's ratio equal to 0,5 can lead to numerical problems as all terms of the stiffness matrix become infinite (Potts & Zdravkovic, 1999).

On the other hand, drained analysis is considered for sand, in which there is a steady state pore pressure. The stiffness matrix contains the effective constitutive behaviour, based on a drained Young modulus, *E'*, and a drained Poisson's ratio, *v'* (Potts & Zdravkovic, 1999). The water is normally dissipated in the case of the loaded sand, hence it is called drained. It is also common to set Poisson's ratio equal to 0,2 – 0,3 in practice.

3.4 PR Technique

Engin (2013) introduced 'Press-Replace' (PR) Technique, which is adopted from Andersen et al. (2004) who modelled penetration of a suction pile in clay. PR Technique uses displacement controlled instead of load controlled scheme. In the PR Technique, the initial FE mesh is preserved. The material properties of the penetrated volume are updated at the beginning of each phase resulting in a change of the global stiffness matrix without the need for a mesh update. Hence, the calculations are relatively fast compared to other algorithms with mesh updating schemes. The PR Technique involves a step-wise updated geometry, which consists of a straining phase followed by a geometry update. During the geometry update, the zone of displaced soil is then replaced by the pile

material. In Figure 3-7, a general view of the model and four subsequent calculation phases are presented. The penetration of the pile (indicated by the darkest colour) can be also seen in the same figure.

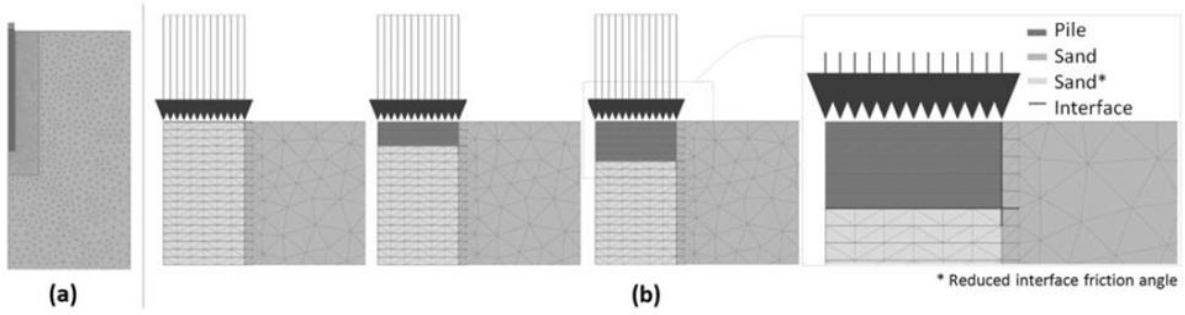

Figure 3-7 Details on a) the Press-Replace modelling technique and b) the progress of penetration of the pile (Engin, 2013).

According to Engin (2013), the purpose of the geometry update is also to model the advancing part of the penetrating object, which can be achieved by modifying the global stiffness matrix at the beginning of every replacement phase (*step 0*). Stage construction process (multiple phases) is resembled in this technique. Therefore, in each phase (*ph*), an updated global stiffness matrix, K^{ph} can be formed.

$$K^{ph}\Delta u^{ph} = \Delta f^{ph} \tag{3-10}$$

The load increment Δf^{ph} is equal to the total unbalance at the beginning of the phase, as a result of the geometry update:

$$\Delta f^{ph} = f_{ext}^{ph} - f_{int}^{ph,0} \tag{3-11}$$

f_{ext}^{ph} is the external load vector at phase *ph* and $f_{in}^{ph,0}$ is the internal reaction vector at the beginning of the phase *ph*.

$$f_{in}^{ph,0} = \int B^T \sigma^{ph,0}\, dV \tag{3-12}$$

B^T is the matrix containing the derivatives of the interpolation (shape) functions and $\sigma^{ph,0}$ is the stress state at the beginning of the phase which is equal to the stress at the end of the previous phase (*ph-1*). The total unbalances forces of the phase Δf^{ph} is solved in multiple steps to obtain accurate solutions. In each step (*i*), the global system is, as follows:

$$K^{ph}\Delta u^{ph,i} = \Delta f^{ph,i} \tag{3-13}$$

$$\Delta f^{ph,i} = f_{ext}^{ph,i} - \int B^T \sigma^{i-1}\, dV \tag{3-14}$$

The use of prescribed displacement as a *Dirichlet* boundary condition will be performed with the solution of the global system equation. Potts and Zdravkovic (1999) explained the procedures on how to impose the prescribed displacement to the global system matrix and to calculate all the displacements and reaction forces.

The total unbalance of each step is also iteratively checked to satisfy the force equilibrium condition. If it meets the tolerance, then the displacement can be updated:

$$u^{ph,i} = u^{ph,i-1} + \Delta u^{ph,i} \tag{3-15}$$

$\Delta u^{ph,i}$ is the displacement of the current step. This calculation procedure is then applied until the desired penetration depth. It should be drawn into attention too that PR Technique is carried out within the framework of small deformation theory, the global stiffness matrix is always formed based on the undeformed geometry of the soil – penetrating object model.

3.5 Parametric study

Various soil properties are taken for the parametric study. The choice of soil properties are mainly based on literature reviews. In this study, values of uniform and increase of clay stiffness ratio, for both homogeneous and non-homogeneous clay, are set between E/s_u= 350 and E/s_u= 500. These ratios fall within the expected range for soft clay and stiff clay (Budhu, 2011).

Unlike penetration in clay, Young modulus has a significant effect once spudcan penetrates into sand layer. The parametric study investigates penetration on loose sand, medium dense sand, and loose sand overlying clay. Table 3-1 shows representatives values of the Young Modulus used as a reference in the present research.

Table 3-1 Representatives values of Young Modulus for sand (Das, 2010).

Soil Type	E_s [kN/m^2]	φ [^{o}]
Loose sand	10,000 – 28,000	25-30
Medium dense sand	28,000 – 35,000	30-35
Dense sand	35,000 – 70,000	35-40

A pressure-dependent Young modulus is adopted in this study. The increase of Young modulus over the depth can be calculated using Janbu approach. Fellenius (2016) presented direct conversion between Young modulus and effective stress. It is expressed, as follows:

$$E = m\,\sigma_r\,(\frac{\sigma'}{\sigma_r})^{1-j} \tag{3-16}$$

Where m is the modulus number, which varies from 100 - 150 for loose sand and 150 - 250 for medium dense sand, σ_r is the reference stress which is equal to 100 kPa, and j is the stress exponent, often taken as equal to 0.5 for sand. Based on Equation 3-16 and Table 3-1, a linear pressure-dependent of Young modulus can be estimated and used as an input in PLAXIS. Hence, the increase of the stiffness with depth (E_{inc}) in the present study are set to be 1000 kN/m^2/m and 1600 kN/m^2/m for loose and medium dense sand correspondingly.

The selection of other parameters, such as s_u, φ, *and* ψ, will be discussed in the next chapter together with the result and discussion for each penetration case.

3.6 The application of PR Technique

The method proposed by Engin (2013) is used for all the analyses in this study. In order to facilitate the PR Technique, an axisymmetric FE mesh with small slices (i.e. $t_s \approx B/8 - B/10$, where B is the spudcan diameter) is introduced in the region where the spudcan will be jacked. It is noted that the use of coarse mesh with 15-node elements is recommended when the PR Technique is employed (Engin et al., 2015).

In using the PR Technique, the simulation should start when the full contact between the spudcan and soil is already established – see Figure 3-8(a). Hence, the spudcan penetration depth, d, in the numerical analyses is defined as zero after the cone completely penetrates into the soil. The penetration process is simulated by several phases of prescribed vertical displacement ($u_y = t_s$) of an idealized circular disc representing the maximum diameter of the spudcan.

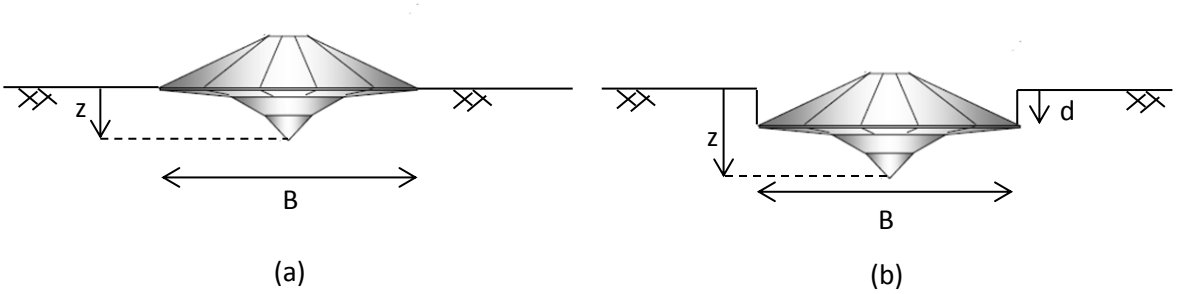

Figure 3-8 Schematic diagram of the spudcan penetration.

Each phase is a small deformation analysis starting from the penetration at the end of the previous phase and the location of the spudcan is updated in each phase (Engin et al., 2015). Figure 3-9 shows how PR Technique is employed for spudcan penetration process in the present study. Interface elements are also defined to model proper interaction between spudcan and soil (*dark green line*), which extend slightly (*black line*) into the soil as suggested by van Langen and Vermeer (1991). Engin et al. (2015) reported that no distinct influence of the interface extension length on the overall behaviour was observed. Hence, for practical reasons, the vertical and horizontal interface extension lengths are equally set to the slice thickness in the analyses.

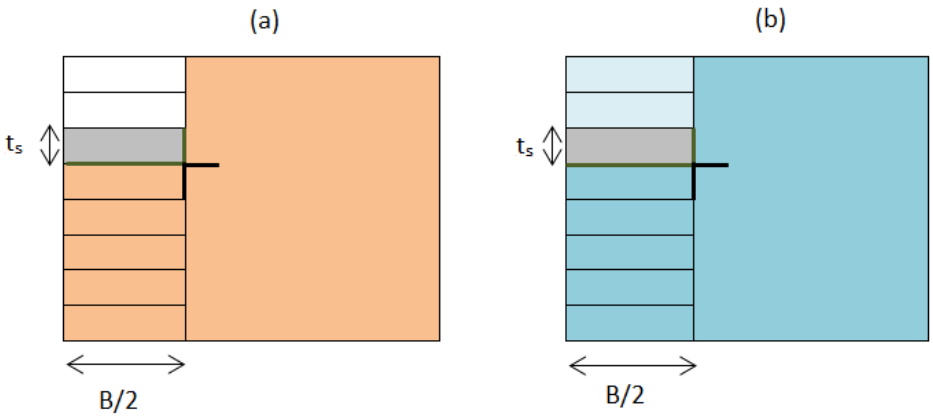

Figure 3-9 PR Technique for spudcan penetration (a) penetration in clay; (b) penetration in sand.

The light grey cluster in Figure 3-9 represents the spudcan body, which is linear elastic. This material model is often used to represent pile, concrete, or other stiff volumes. Young modulus of 200 GPa and Poisson's ratio of 0.3 are adopted to model the spudcan.

Engin (2013) also reported the challenges on choosing the appropriate interface stiffness and strength, especially for the interface extensions. Those suggestions are also applied in the current study. High strength and stiffness values are assigned to the interface extensions for penetration in sand to ensure that the extended interfaces do not fail or deform (e.g. c_{ref}= 10 MPa, E_i = 500 E_{soil}). For penetration in clay, 5 times stronger ($s_{u,i}$ = 5 $s_{u,soil}$) and 10 times stiffer (E_i = 10 E_{soil}) than adjacent soil are applied for the interface extensions properties.

The simulations follow the "wished-in-place" method by removing all soils within the plan area of the spudcan down to the base level (see again Figure 1-3). For penetration in clay, this cavity can be maintained in the region above the spudcan for all the investigated cases in this study. As discussed in the previous chapter, according to the experimental test conducted by Hossain (2008), there would be a critical or maximum cavity depth due to the backflow mechanism as the soil flows back and provide seal on top of the spudcan (Figure 2-4). However, Engin et al. (2015) emphasized that backflow mechanism cannot be captured by the PR Technique. It is expected that the result obtained using PR Technique would not be too accurate when the penetration depth exceeds the critical cavity depth.

In contrast, for the penetration in sand, sand material has to be placed above the spudcan to avoid numerical failure in PLAXIS. That soil cluster is assumed to have the same properties as the adjacent soil, but with lower stiffness (1/2 *E'* of the surrounding soil).

In the case of penetration in double layer system, slices of thickness (t_s) of an axisymmetric FE mesh are defined compatible to the layering, sand thickness, and not equal to a predefined value as mentioned in the beginning of this subchapter.

3.7 Conclusion

Some aspects, such as constitutive model, mesh size, boundary condition, and interface elements, have been briefly covered in this chapter. The technique and framework described in this chapter are used for all numerical analyses in the current study. Additional explanation might be added in the next chapters if necessary.

Chapter 4.
Penetration in Single Layer

This chapter shows the results of the numerical simulations of spudcan penetration process into sand, homogeneous clay, and nonhomogeneous clay. The first section of this chapter will present the comparison between the present study and centrifuge test or numerical results carried out by other researchers. The effects of mesh density and step size are also studied. After which, the influences of boundary distance and interface elements are explored. A parametric study on different diameters and soil properties is carried out to investigate the penetration curve of spudcan foundation in a single layer. The spudcan penetration depth, *d*, in the numerical analyses is defined as zero after the cone completely penetrates into the soil. Dividing the total vertical reaction by the widest spudcan area will give the bearing pressure, *q*.

4.1 Comparison

4.1.1 Penetration in sand

One case is simulated according to numerical analysis presented by Qiu et al. (2010). Spudcan with 14m of diameter penetrates into dense sand (relative density, *RD*= 80%) with a friction angle of 31.5^{o}. The effective unit weight of sand is set to be 11 kN/m^{3}. Based on Table 3-1 and equation 3-16, the increase of the stiffness with depth (E_{inc}) is assumed to be 2500 kN/m^{2}/m. Using formula provided by Brinkgreve et al. (2010), dilatancy for the sand layer can be estimated and found to be 8^{o} based on the given relative density.

$$\psi = -2 + 12.5\,RD \;\; [^{o}] \tag{4-1}$$

The simulations are performed by keeping the bottom boundary at 10*B* from the domain surface. The lateral domain boundary is also kept at a distance of 10*B* from the centre of the spudcan. The results are plotted in Figure 4-1(b) and also compared with the results obtained by Qiu et al. (2010).

Since the PR Technique is based on straining and material switch, it is important to know the effect of the step size or the penetration length at each phase. The comparison of having two different mesh densities named coarse and medium mesh is also presented in this section. All cases are observed and summarized in Table 4-1 and Figure 4-1(a).

Table 4-1 Summary of analysis for the investigation of step size and mesh density (sand).

Case	Slice thickness/step size (u_y= t_s)	Mesh density
E1c	1 m	Coarse
E1m	1 m	Medium
E2c	1.25 m	Coarse
E2m	1.25 m	Medium
E3c	1.5 m	Coarse
E3m	1.5 m	Medium

Furthermore, the soil-spudcan interface strength in all the simulations mentioned above are assumed in the order of 0.7 (R_{inter} = 0.7) since no detailed information can be obtained. In general, for real soil-structure interaction the interface is weaker and more flexible than the surrounding soil,

which means that the value of R_{inter} should be less than 1 as also recommended by Brinkgreve et al. (2015).

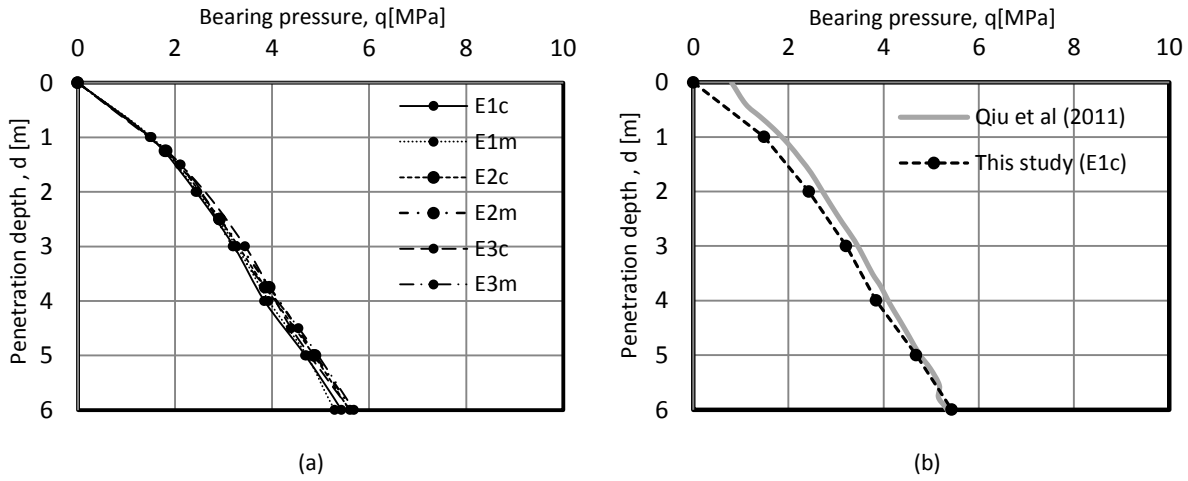

Figure 4-1 (a) Spudcan penetration curves with varied step sizes and mesh densities (sand); (b) Comparison to other the solution from Qiu et al. (2010).

In Figure 4-1(a), an acceptable (max. 4.5%) difference in bearing pressure values is obtained. The bearing pressure predicted by PR Technique shows a similar trend to the result predicted by Qiu et al. (2010) using CEL method in Abaqus, as can be seen in Figure 4-1(b). The bearing pressure obtained from PR Technique is initially lower than that predicted by CEL method. However, both approaches converge to $q \approx 5.4$ MPa as the spudcan penetrates deeper (d= 6m). The difference might be due to the soil properties such as dilatancy and Young modulus that are assumed in the simulation.

4.1.2 Penetration in clay

Hossain (2008) reported a LDFE analysis of a spudcan with a diameter of 18m. Some prescribed parameters for this case are: s_u= 200 kPa; γ'= 10 kN/m^3; v= 0.495; E/s_u= 500. PR Technique is performed to recalculate the case investigated by Hossain (2008). The boundary distance is kept at a distance of 10B from the reference axis. The influence of slice thickness and mesh density is also investigated, with a similar set-up as presented in Table 4-1. The results are plotted in Figure 4-2 and compared to the results obtained by Hossain (2008) and other solutions, see Figure 4-3.

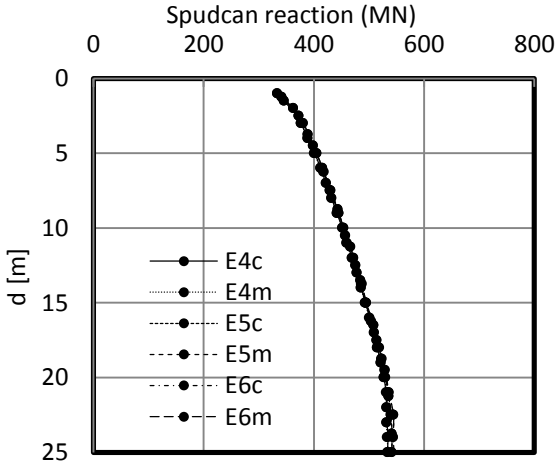

Figure 4-2 Spudcan penetration curves with varied step sizes and mesh densities (clay).

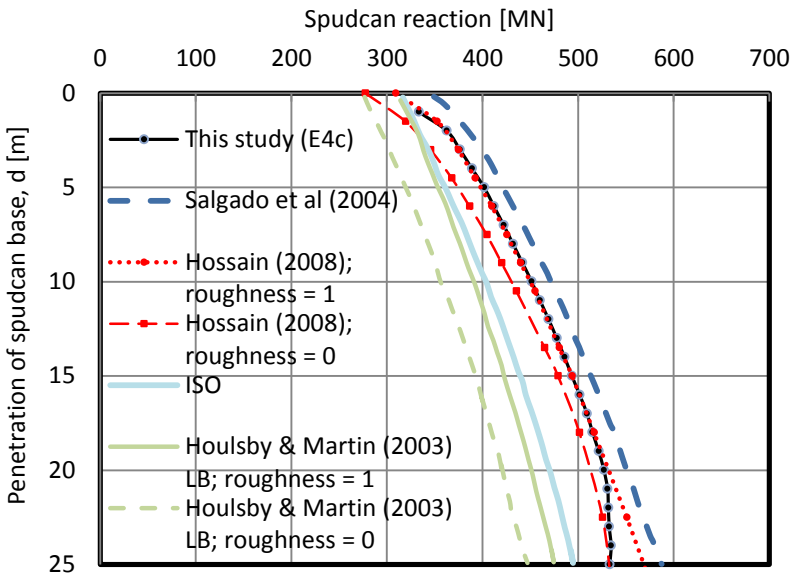

Figure 4-3 Comparison to other the solution, after Hossain (2008).

There is no significant difference in spudcan reactions observed in changing the step size and mesh density, as can be seen in Figure 4-2. The spudcan reaction predicted by PR Technique (E4c) is plotted in Figure 4-3 and shows similar trend line to other solutions that were presented in Hossain (2008). In this extreme case with s_u= 200 kPa, the cavity situation above the spudcan is assumed as "fully-open" without any backflow. This example is picked as a comparison since PR Technique employed in this study also keeps the cavity open in all analyses. The PR Technique's solution is bracketed between two results, using the proposed equations by Hossain (2008). The change of slope is observed at penetration around 20m. This might be due to the change of flow mechanism. This issue will be discussed in subchapter 4.3.

The procedure described in the ISO guideline use the "wished-in-place" method for analyzing spudcan resistance based on the framework of onshore foundation. The approach uses the bearing capacity factors based on solutions for a strip footing with the depth and shape factors by Skempton (1951). The N_c values by Skempton (1951) do not account for an increase in strength over the depth. ISO also gives an alternative method by applying N_c values proposed by Houlsby and Martin (2003) which are based on a curve fit that accounts for embedment, cone angle, rate of increase of strength with depth, and spudcan roughness. The dark blue line in Figure 4-3 uses the upper bound of bearing capacity factors proposed by Salgado et al. (2004). Different values of depth and shape factors based on the finite element analysis are incorporated in the calculation. The estimation by Hossain (2008) is based on a large deformation analysis that can capture more than adequately the soil flow mechanism (including backflow) in continuous penetration of the spudcan. Some aspects such as, simplification of the spudcan geometry and limitation to capture soil flow mechanism, might lead to the difference between PR Technique and other solutions.

4.2 Boundary distance effect

Finite element analysis employing PR Technique is used in this section to explore the effect of the lateral and bottom boundary effect of the soil domain. According to Ullah et al. (2016), L_{BD}= 10B can be taken as a reference case without the effect of the boundary condition on penetration response since no significant difference can be observed with a more distant boundary. For a practical reason,

the lateral boundary distance is always set to be equal to the bottom boundary distance (L_{BD}= B_{BD}= BD).

For uniform sand, *BD* is varied from 10*B* to 4*B*, while case with *BD* of 3*B* is added for penetration in uniform clay. Loose sand with a friction angle of 30^o is used in all analyses, with some prescribed parameters such as v= 0.3, ψ= 0^o, γ'= 11 kN/m^3, and E_{inc}= 1000 kN/m^2/m. Uniform undrained shear strength of 50 kPa and uniform stiffness ratio, E/s_u= 350 are applied for the clay in all analyses. The effective unit weight of clay is taken as 10kN/m^3 and the Poisson's ratio is set to be 0.495.

Table 4-2 Case study for boundary effect (S = Sand; C= Clay).

Case	B [m]	φ [^{o}]	s_u [kPa]	R_{inter}	BD
S – BD 1	10	30	-	0.7	10B
S – BD 2	10	30	-	0.7	8B
S – BD 3	10	30	-	0.7	6B
S – BD 4	10	30	-	0.7	4B
C – BD 1	10	-	50	0.7	10B
C – BD 2	10	-	50	0.7	8B
C – BD 3	10	-	50	0.7	6B
C – BD 4	10	-	50	0.7	4B
C – BD 5	10	-	50	0.7	3B

All the analyses for investigating the boundary distance effect are summarized in Table 4-2 and the results can be seen in Figure 4-4. Figure 4-4 reveals that reducing the boundary distance has a minimal impact in the load penetration response for spudcan penetration in uniform clay. The soil flow mechanism is gradually localized with further penetration in clay. Hence, the effect of boundary distance is negligible. In contrast, significant increase of the bearing pressure can be seen in uniform sand, e.g. *BD*= 4*B*, as the sand becomes stronger with depth and stress perturbations are propagated over a larger distance than that in clay. When the boundary is close to the spudcan, the lateral movement of sand is restricted and the soil tends to move upwards, resulting in a higher resistance.

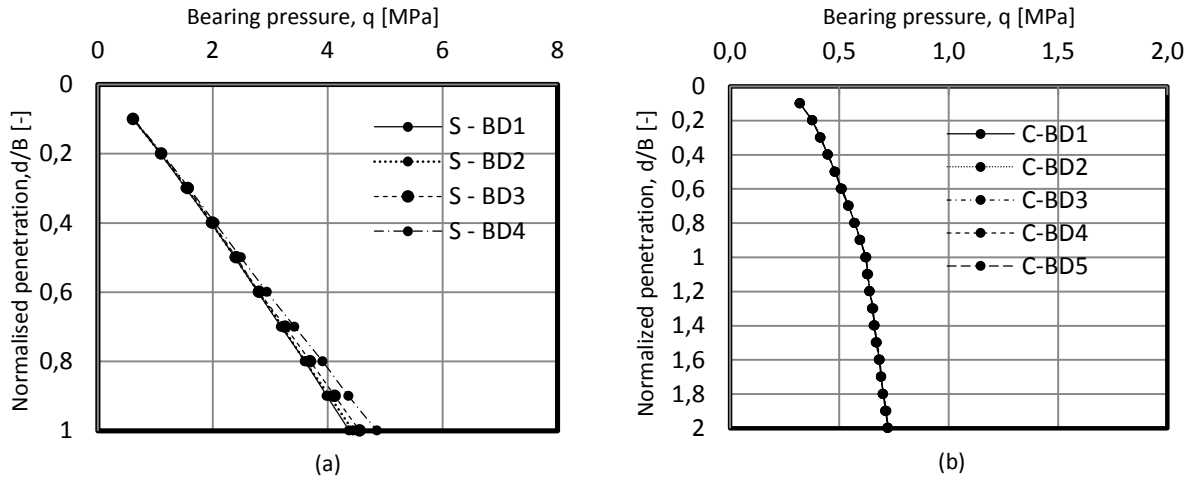

Figure 4-4 Spudcan penetration curve with various boundary distance in (a) sand (b) clay.

4.3 Young modulus and interface elements

This section investigates the effect of Young modulus and interface elements in the numerical simulations. Loose sand with a friction angle of 30° is used in all analyses, with some prescribed parameters such as v= 0.3, ψ= 0°, and γ'= 11 kN/m^3. Using Equation 3.16 and Table 3-1, E_{inc} can be varied as can be seen in Table 4-3. For penetration in clay, constant parameters are set: γ'= 10 kN/m^3; v= 0.495; s_u= 50 kPa. Table 4-3 shows all the case study in this section.

Table 4-3 Case study for Young modulus effect (S = Sand; C= Clay).

Case	B [m]	E_{inc} [kN/m^2/m]	R_{inter}	BD
S – Y1	10	1000	0.7	10B
S – Y2	10	650	0.7	10B
S – Y3	10	700	0.7	10B
S – Y4	10	770	0.7	10B
S – Y5	10	900	0.7	10B
Case	**B [m]**	**E/s_u**	**R_{inter}**	**BD**
C – Y1	10	350	0.7	10B
C – Y2	10	300	0.7	10B
C – Y3	10	250	0.7	10B
C – Y4	10	400	0.7	10B
C – Y5	10	450	0.7	10B
C – Y6	10	500	0.7	10B

Figure 4-5 shows that having different Young modulus does not modify the penetration curve for the case of uniform clay. Volumetric change is not allowed when using undrained analysis for clay. This implies that the bulk modulus is infinite. Hence, changing the modulus does not have an effect on the resistance, but it is mainly controlled by the undrained shear strength of clay (s_u). On the other hand, increasing or decreasing Young modulus modifies the magnitude in penetration on sand as the spudcan penetrates deeper. The soil has to deform to take the load and the deformation is controlled by the elastic modulus. It can be concluded that the choice of Young modulus plays important role in penetration on sand. For the parametric study, a reference Young modulus discussed in subchapter 3.5 is used for practical reasons.

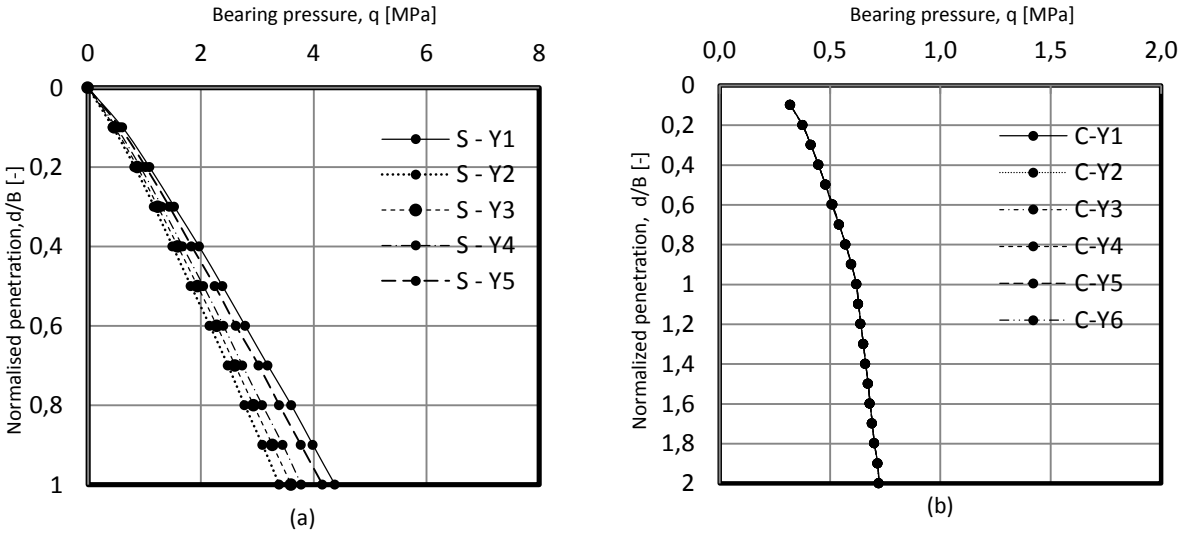

Figure 4-5 Spudcan penetration curve with various Young modulus in (a) sand (b) clay.

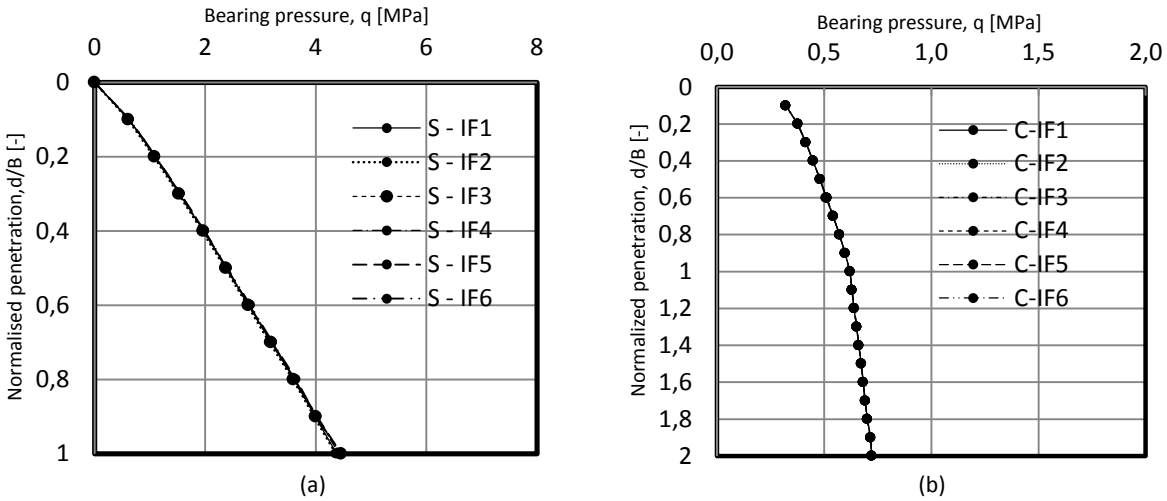

Figure 4-6 Spudcan penetration curve with various R_{inter} in (a) sand (b) clay.

In addition to the Young modulus, the influence of interface element is considered in this section. Interface elements applied in this study are using the linear elastic model with Mohr-Coulomb criterion. The interface properties can be set with a reduction factor, R_{inter}. The default value is R_{inter} = 1, a fully rigid condition.

Figure 4-6 shows the load penetration curves for different R_{inter} ,(i.e. R_{inter}= 0.5 – 1). In general, applying a rigid reduction factor gives a higher bearing pressure. However, there is no notable difference. In this research, the effect of interface properties can be neglected. For further analyses, a factor of 0.7 is applied in all simulations since no detailed information can be obtained, as also explained in subchapter 4.1.1.

Moreover, as observed in the penetration curves of penetration in clay, there is a change of the slope in bearing pressure. This happens at $d/B \approx 1$, with s_u= 50 kPa and γ'= 10 kN/m^3. This change might be caused by the variation of the flow mechanism that is depicted in Figure 4-7. Once the spudcan penetrates further, e.g. $d/B \approx 1$, localized soil flow occurs without any surface movement. This can be called deep penetration.

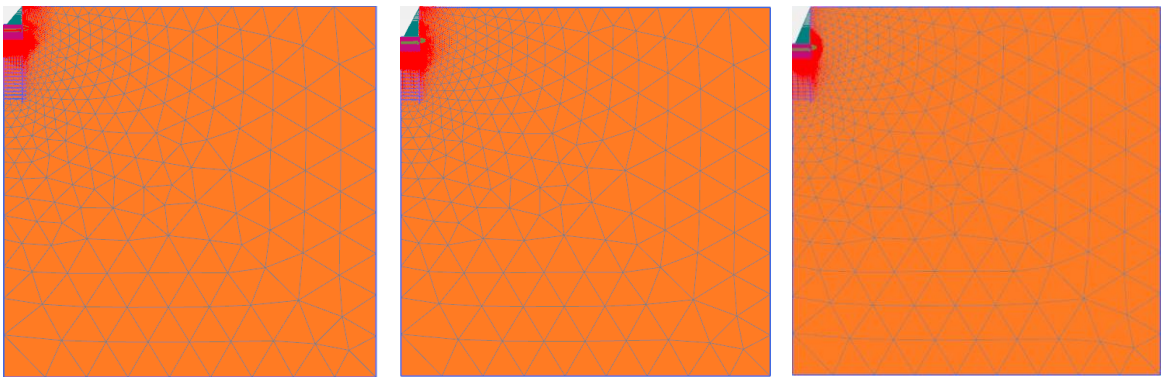

d/B= 0.5 d/B= 0.75 d/B= 1

Figure 4-7 Flow mechanism of spudcan penetration in clay.

4.4 Parametric study

A parametric study is carried out for both penetration in sand and clay. In all analyses, the boundary distance is kept at a distance of 10B from the reference axis. The cases are briefly mentioned in the following subchapters. The summary of all cases is presented in Appendix A. Chapter 3.5 is used as a reference in order to classify the soil and determine some soil properties.

4.4.1 Sand

The main focus of the parametric study of penetration in sand lies on the influence of the foundation diameter, the friction angle, and the effect of dilatancy on the bearing capacity of the footing. According to Budhu (2011), the dilatancy angle has values ranging from 0^0 to 15^0 and the influence of dilatancy angle is only parametrically explored for medium dense sand.

The cases in this section are listed below:

a. *Spudcan geometry: B*= 5, 10, 15 m.
b. *Friction angle: φ*= 25^0, 27^0, 29^0 (loose sand); 30^0, 32^0, 34^0 (medium dense sand).
c. *Dilatancy angle: ψ*= 0^0, 5^0, 10^0, 15^0.
d. *Effective unit weight: γ'*= 11 kN/m^3.

4.4.1.1 Non-dilative sand

Firstly, parametric study is done for non-dilative sand by setting the dilatancy angle equals to zero. The analyses are done for both loose sand and medium dense sand.

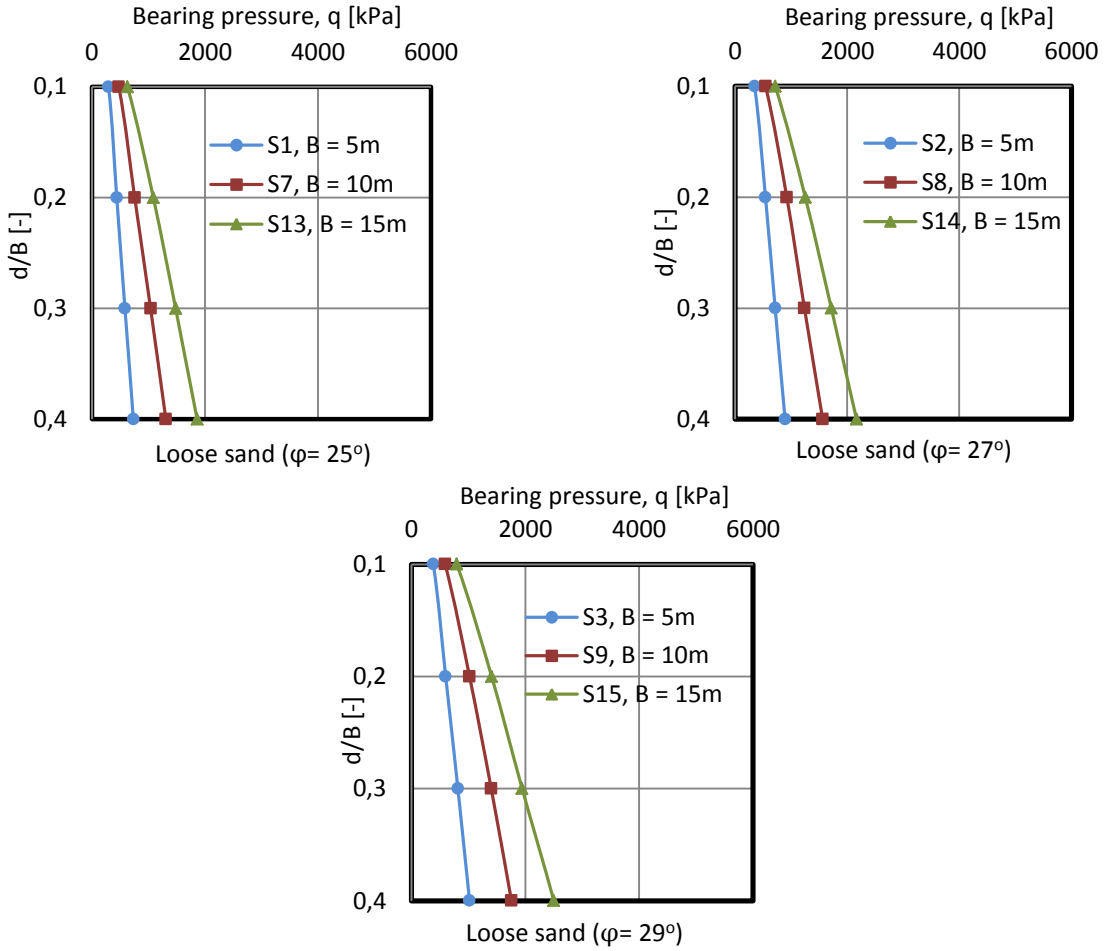

Figure 4-8 Bearing pressure of the spudcan penetrating into loose sand.

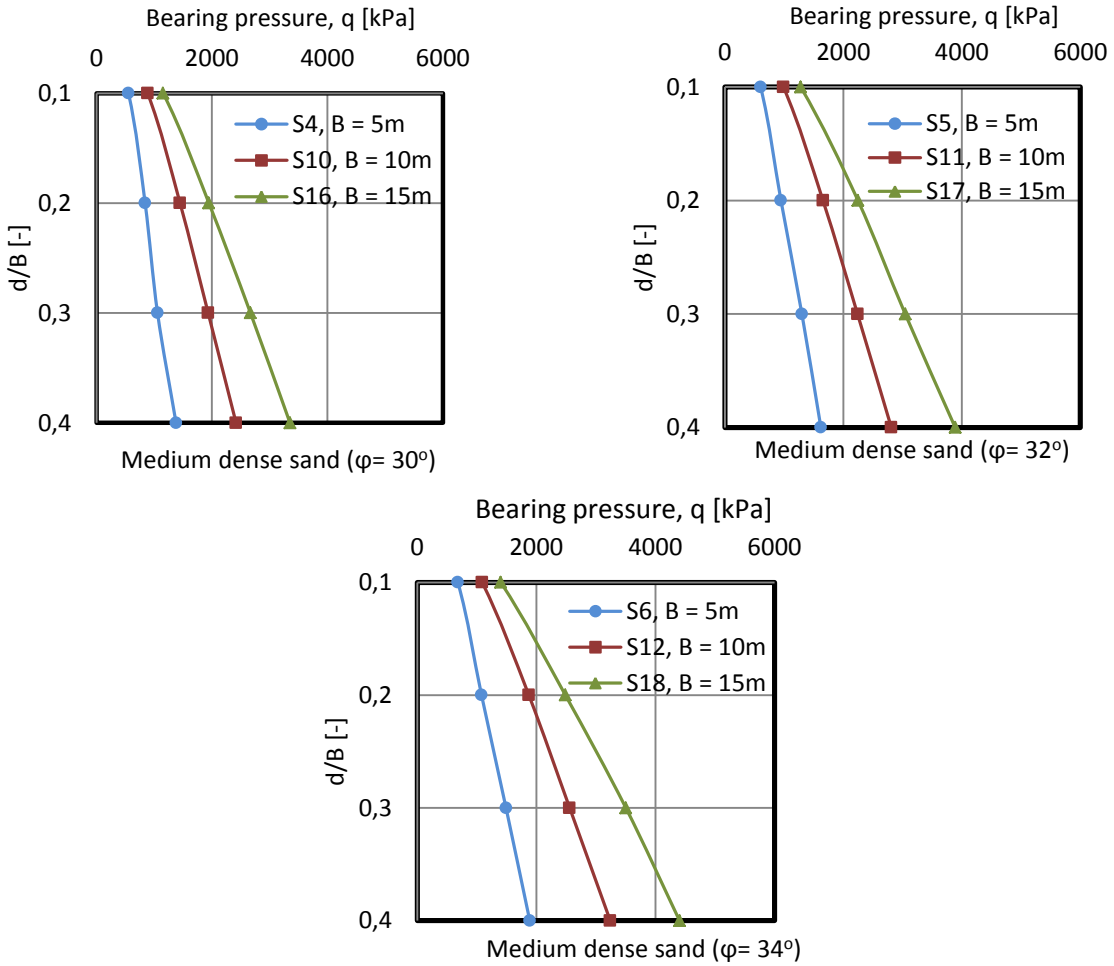

Figure 4-9 Bearing pressure of the spudcan penetrating into medium dense sand.

In Figure 4-8 and Figure 4-9, the bearing pressures of spudcans with different diameters and friction angles are depicted over the normalized penetration depth. The axis scale in both figures is the same. It is evident that the bearing pressure increases with increasing spudcan diameter and friction angle. The bearing pressure can also be shown as a dimensionless pressure, which corresponds to the bearing capacity factor, N_γ (see equation 2-1 until 2-4), N_γ is the contribution of the unit weight of the soil to the bearing capacity. The rearrangement of equation 2-1 leads to the following equation:

$$N_\gamma = \frac{q - \left\{exp^{\pi \tan(\varphi)} tan^2\left(45^o + \frac{\varphi}{2}\right)\right\} \gamma' d}{\gamma' B/2} \tag{4-2}$$

Using this normalization, the influence of spudcan diameter can be better investigated. Figure 4-10 depicts the dimensionless bearing pressure for the cases of non-dilative sand. Besides the dependency on the friction angle, φ, it can be noted too that the bearing capacity factor, N_γ, decreases with increasing spudcan diameter. Table 4-4 shows examples of N_γ values obtained from the investigated cases.

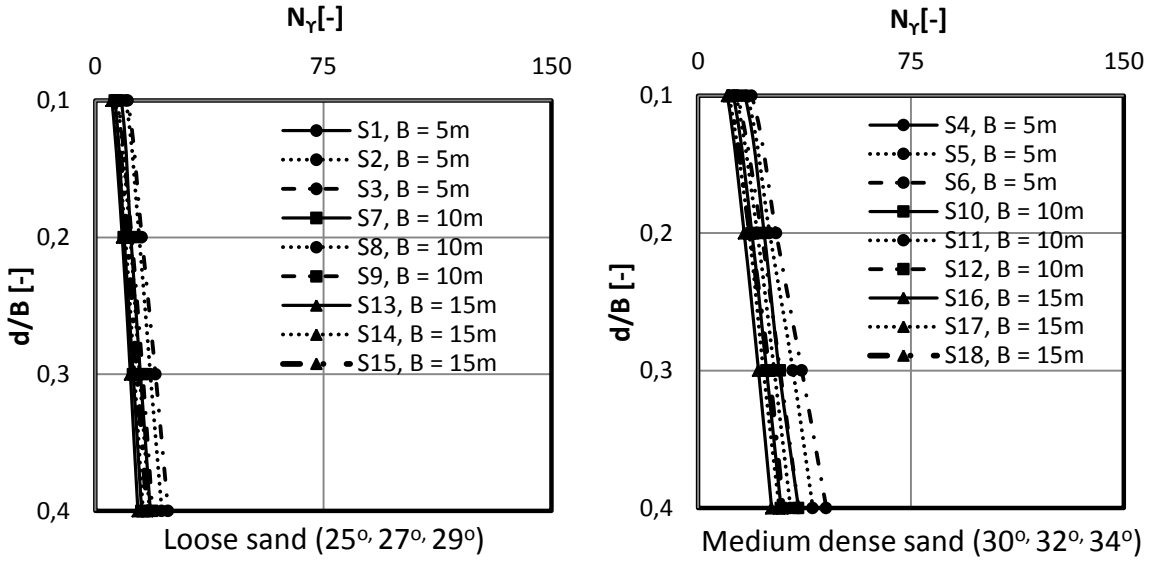

Figure 4-10 Normalized bearing pressure for non-dilative sand.

Table 4-4 Values of N_γ from the present study at d/B= 0.1.

	N_γ		
φ [°]	**B= 5m**	**B= 10m**	**B= 15m**
25	8.597	6.518	5.504
30	16.474	12.422	10.296

In the PR Technique, the conical underside of the spudcan is not modelled. Hence N_γ cannot be obtained directly when d/B= 0 since the load is zero. The bearing pressure at d/B= 0.1 is used instead (White et al., 2008). As can be seen in Table 4-4, although the difference in bearing capacity factor is not big, it clearly shows the N_γ decreases with increasing footing diameter. White et al. (2008) also discussed this issue, and this reduction of N_γ is called *stress-level effect*. This effect arises because the mean in situ stress level, often taken as $\gamma' B/2$, within the failure mechanism is related to the diameter of the foundation.

Although several researchers, for instance Zhu et al. (2001), White et al. (2008), and Yamamoto et al. (2009), have shown that the N_γ is found to reduce with increasing foundation size, the bearing capacity factors in the industry guidelines are still given merely as a function of friction angle. For this reason, the accuracy of predicting spudcan penetration in the current industry guidelines can still be improved.

4.4.1.2 Dilative sand

The volume of granular soil might increase during shear, this volume increase is also known as dilatancy. Dilatancy is characterized by a dilatancy angle, ψ, that is related to the ratio of plastic volumetric change to the plastic shear strain. The influence of dilatancy angle on the penetration response is looked in this section. The analysis is only done for medium dense sand since it is commonly known that dilatancy does not play a role in loose sand.

Figure 4-11 depicts the bearing pressure of spudcan penetrating in medium dense sand with different footing diameters and dilatancy angles. The bearing pressure increases with increasing dilatancy angle. The effect of dilatancy is also more prominent for sand with a higher friction angle. Hence, it is obvious that dilatancy angle will then have a significant influence on the bearing capacity factor, N_γ. Figure 4-12 might explain the influence of dilatancy angle. In general, with increasing ψ, larger displacement occurs, especially in the region next to the footing edge and the sand tends to move upwards with the higher value of dilation angle, resulting in a higher penetration resistance.

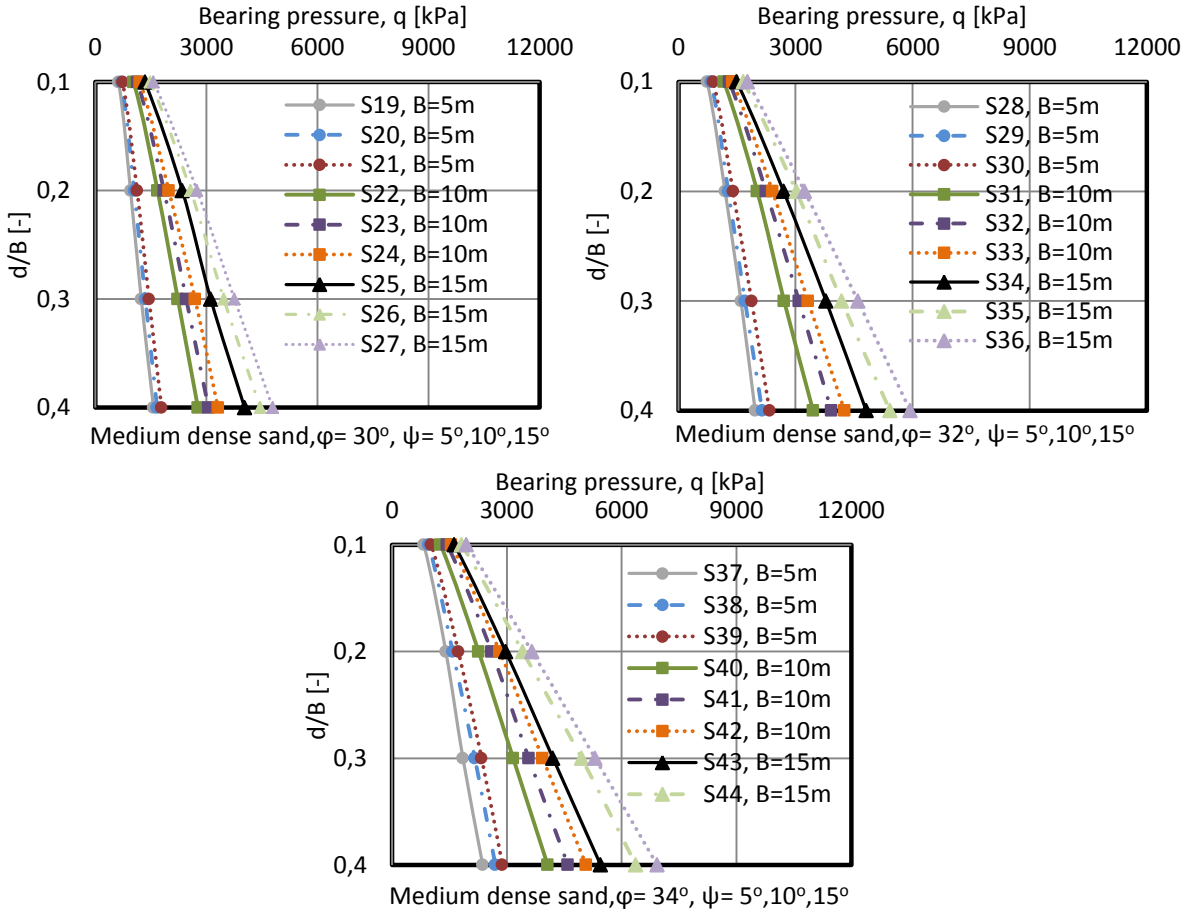

Figure 4-11 Bearing pressure of the sudcan penetrating into medium dense sand – influence of dilatancy.

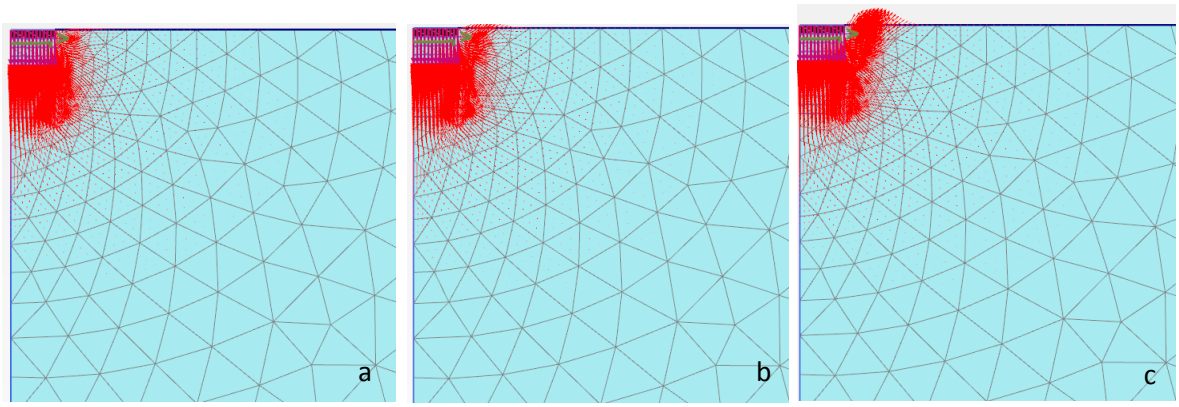

Figure 4-12 Displacement field for φ= 30° with (a) ψ= 5°; (b) ψ= 10°; (c) ψ= 15°.

Although the traditional bearing capacity equations presented in subchapter 2.2 seems to be independent of dilatancy angle, the solutions are actually formulated with assuming that the soil follows an associated flow rule, this means that the dilatancy angle, ψ, equals to the friction angle, φ. In reality, it is commonly known that the dilatancy angle is lower than the friction angle. According to Budhu (2011), the dilatancy angle has values ranging from 0^0 to 15^0. It has been suggested that the traditional bearing capacity equation can be extended to include the effect of non-associativity ($\psi < \varphi$) by applying a reduced friction angle, φ^* (Lee, 2009). The approach suggested by Drescher and Detournay (1993) can be used to modify the friction angle for soils following a non-associative flow rule:

$$\tan\varphi^* = \frac{\sin\varphi\cos\psi}{1-\sin\varphi\sin\psi} \tag{4-3}$$

A slightly different approach is used to normalize the bearing pressure. The reduced friction angle, φ^*, obtained by using equation 4.3 is then inserted to the equation 4.2 to find N_γ.

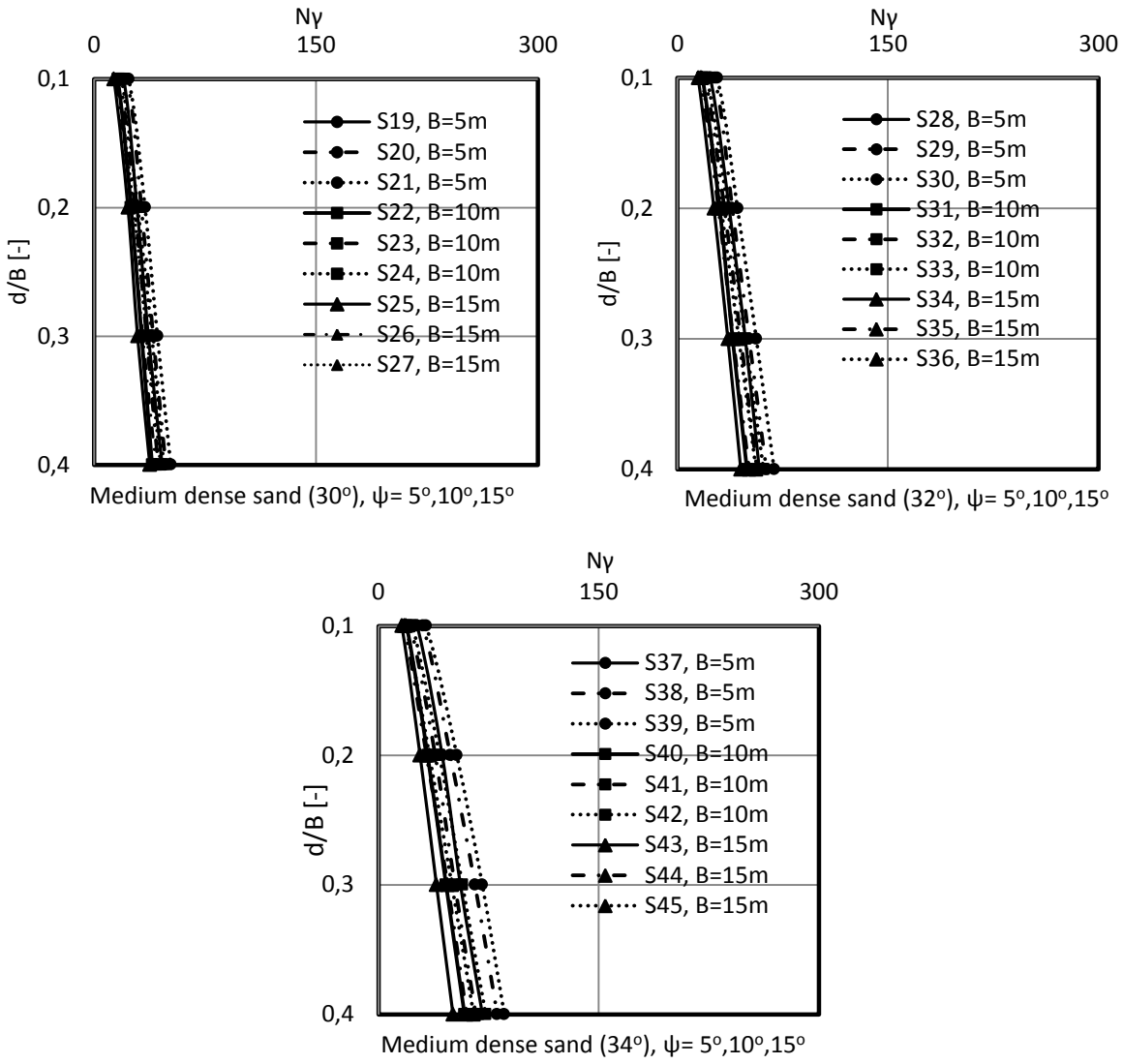

Figure 4-13 Normalized bearing pressure for dilative sand.

Figure 4-13 shows the normalized penetration curves for medium dense sand. It can be seen that the effect of dilatancy becomes more prominent for sand with a higher friction angle since the normalized bearing pressure chart is less converged, e.g. $\varphi = 34^{o}$. N_γ also still depends on the spudcan diameter.

Finding the exact solution of N_γ is not the objective of this study and might not be accurate using the constitutive soil model that is applied in the present research. Figure 4-14 shows the volumetric behaviour of dense sand. It shows that the soil will reach a critical state at some point and further shear deformation will occur without volume changes (Brinkgreve et al., 2015). In the Mohr-Coulomb model, a contant dilatancy angle is applied. This implies that the soil will continuously dilate as long as shear deformation occurs. Therefore, the end of dilatancy, as generally observed when the soil reaches the critical state cannot be modelled using the Mohr-Coulomb constitutive soil model.

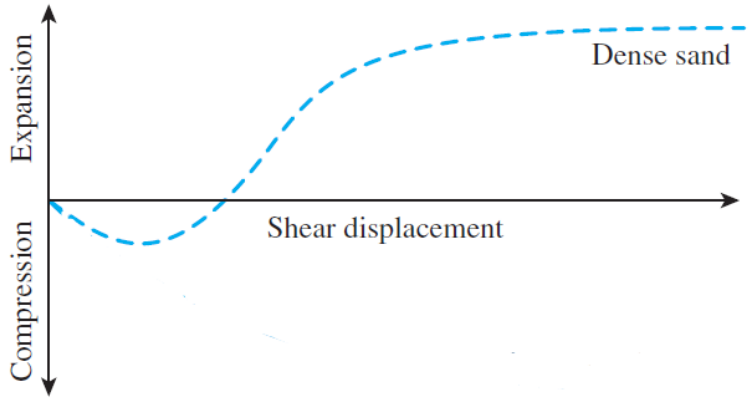

Figure 4-14 direct shear stress for dense sand (Das, 2010).

Loukidis and Salgado (2009) proposed N_γ and N_q factors that account for the effect of the dilatancy angle. Using these bearing capacity factors for spudcan penetration, however, needs further study since the research by Loukidis and Salgado (2009) was carried out for strip and circular footings that are resting on the soil surface. In the case of spudcan penetration, the embedment depth should be taken into account as the spudcan penetrates further into the soil.

For the present study, it is concluded that the effect of non-associativity ($\psi < \varphi$) on the bearing capacity of spudcan foundation is not negligible. As a result, calculating the bearing capacity that follows non associative flow rule would give difference results compared to the solutions provided by the industry guidelines. In practice, a proper value of dilatancy angle, that is normally obtained from laboratory test, should be used when using finite element program to assess spudcan penetration on sand.

4.4.2 Clay

4.4.2.1 Homogeneous clay (k= 0 kPa/m)

Uniform clay is used as a starting point since spudcan penetration solutions provided by industry guidelines are generally formed by studies of foundations on uniform clay. The selection of parameters in this study is based on Hossain (2008) that carried out a survey throughout case histories and offshore geotechnical reports in order to select realistic soil parameters. The investigated cases in this section are listed below:

a. Spudcan geometry: B = 5, 10, 15 m.

b. Effective unit weight: γ' = 8 and 9 kN/m^3.

c. Normalized strength at the mudline: $s_{um}/\gamma' B$= 0,5 and 1.

Table 4-5 Investigated case for homogeneous clay

Case	B [m]	γ' [kN/m^3]	s_{um} [kPa]	s_{um} / γ'B
C1	5	9	22,5	0,5
C2	10	9	45	0,5
C3	15	9	67,5	0,5
C4	5	9	45	1
C5	10	9	90	1
C6	15	9	135	1
C7	5	8	20	0,5
C8	10	8	40	0,5
C9	15	8	60	0,5
C10	5	8	40	1
C11	10	8	80	1
C12	15	8	120	1

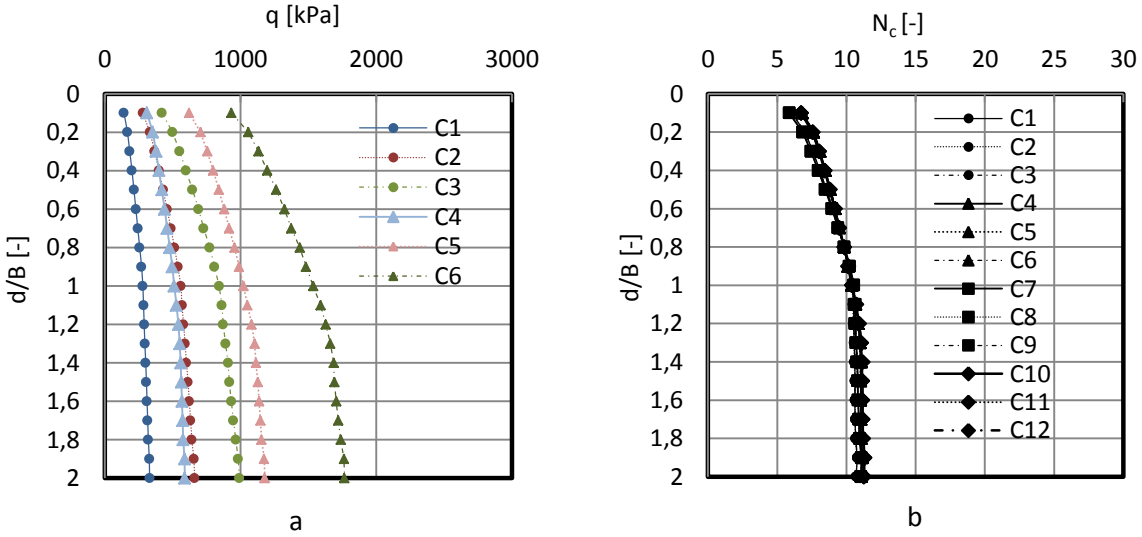

Figure 4-15 Load penetration curves of spudcan penetration in homogeneous clay.

Figure 4-15(a) shows some results of spudcan penetration in homogeneous clay with different diameters and different normalized strength ($s_{um}/\gamma'B$), but with the same effective unit weight. Other results can be seen in Appendix A. The footing resistance is mainly governed by the normalized strength value. Increasing this ratio will result in higher bearing pressure.

Spudcan installation in soil with self-weight causes backflow above the spudcan at a relatively shallow depth (Hossain, 2008). However, due to the limitation of the technique employed in this study, this backflow cannot be captured. The cavity above the spudcan is maintained in all the simulations that may not give accurate result in deep penetration ($d>H_{cav}$ or after backflow occurs).

An attempt is done to normalize the penetration curve, using equation 2-1, that corresponds to the bearing capacity factor, N_c, as can be seen in Figure 4-15(b). As expected, it results to form unique lines. The bearing capacity factor increases with the depth until a normalized penetration depth of about 1.1 - 1.2. Below that depth, the bearing capacity factor becomes independent of the normalized penetration depth and the quantity of $s_{um}/\gamma'B$. This term is denoted N_{cd} to indicate deep penetration (Hossain, 2008).

In contrast to the finding in this study, N_c values observed by Hossain (2008) still increases after d/B= 1.2 and reach deep penetration at deeper depth. This incongruity might be caused by the existence of backflow above the spudcan in LDFE and centrifuge test analysis carried out by Hossain (2008), resulting in the rise of bearing resistance because of the shearing deformations within the backflow soil.

4.4.2.2 Non-homogeneous clay (k≠ 0 kPa/m)

This section deals with the spudcan foundations installation in non-homogenous clay. Offshore clays normally tend to show increasing undrained shear strength with depth. The increase is more or less linear and commonly expressed as:

$$s_u = s_{um} + kd \tag{4-4}$$

The choice of parameters in the present study is also based on the survey done by Hossain (2008). The cases in this section are listed below:

a. *Spudcan geometry: B* = 5, 10, 15 m.
b. *Effective unit weight: γ'* = 7 and 8 kN/m^3.
c. *Gradient of undrained shear strength: k*= 1, 2, 3 kPa/m
d. *Normalized strength at the mudline*: $s_{um}/\gamma'B$= 0.063 to 0.429
e. *Degree of non-homogeneity: kB/s_{um}*= 1 and 2

Setting some parameters as listed above will vary the undrained shear strength ranging from 5 to 45 kPa at the mudline. The effect of changing the footing size and the increase rate of undrained shear strength is noticed in this study. Some cases investigated in this section are tabulated in Table 4-6 and presented in Figure 4-16. Summary of all cases are tabulated in Appendix A. Figure 4-16 clearly shows that increasing footing diameter or the undrained shear strength gradient over the depth, *k*, will give a higher bearing pressure.

Table 4-6 Some investigated cases for penetration in non-homogeneous clay.

Case	B [m]	γ′ [kN/m^3]	k [kPa/m]	kB/s_{um}
C13	5	7	1	1
C19	5	7	2	1
C25	5	7	3	1
C26	10	7	3	1
C27	15	7	3	1

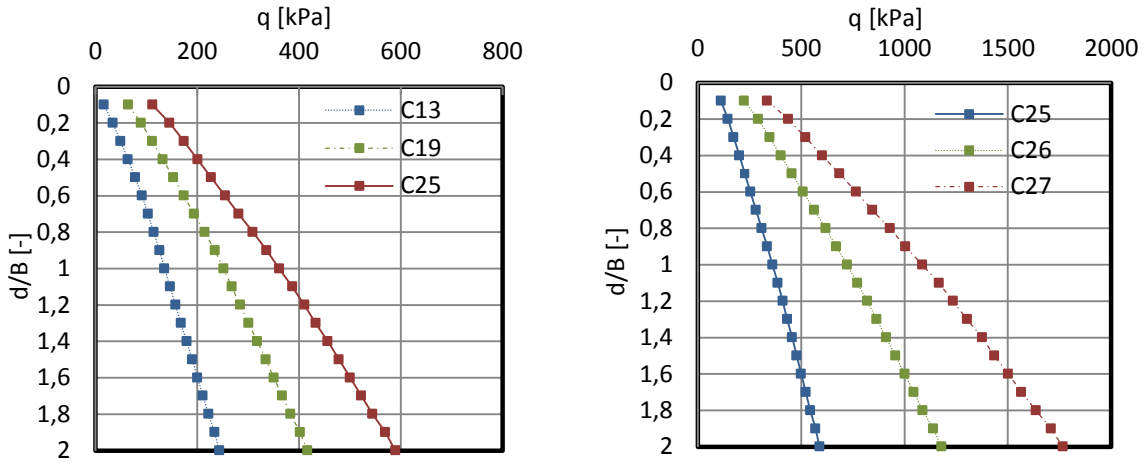

Figure 4-16 Load penetration curves of spudcan penetration in non-homogeneous clay.

As for homogeneous clay, all the results from non-homogeneous clay will be normalized. The penetration depth will be normalized with respect to the footing diameter. Likewise the attempt for homogenous clay, equation 2-1 will be used to obtain the bearing capacity factor, N_c. Figure 4-17 shows all the normalized penetration curves. It should be noted that the curves from penetration analysis in homogeneous clay is also included. The computed N_c agrees well to those analyses for homogeneous clay. N_c gradually increases before reaching the limiting value, N_{cd}, at penetration depth of d/B= 1.1 – 1.2. The same explanation about backflow in 4.4.2.1 might be used.

Hossain (2008) also reported the comparison of small deformation and large deformation analysis for penetration in clay (see Appendix A). It also shows that, using large deformation analysis, N_c increases gradually at shallow penetration and delay the attainment of limiting bearing capacity factor, N_{cd}. Moreover, the N_c values obtained by large deformation analysis are generally lower than the ones by small deformation analysis. It might be due to the existence of the soft soil around the spudcan that is trapped and dragged down from the surface to the embedment level as the spudcan penetrates deeper (Hossain, 2008).

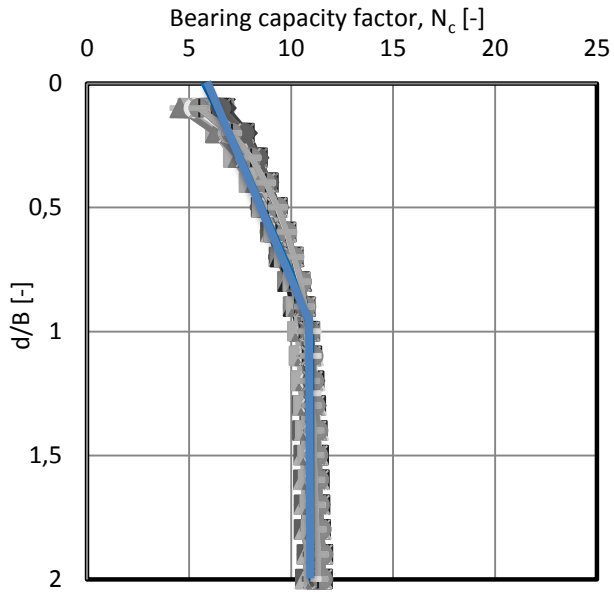

Figure 4-17 Normalized penetration curve for homogeneous and nonhomogeneous clay.

An approximate linear curve of N_c (blue line in Figure 4-17) is proposed for all the investigated cases in this study.

$$N_c = 5.837(1 + 0.914\frac{d}{B}); 0 \leq \frac{d}{B} \leq 1 \quad (4\text{-}5)$$

$$N_c = 11; \frac{d}{B} \geq 1 \quad (4\text{-}6)$$

The proposed curve might only be valid for the parameters used in the present research. More parametric studies are needed so that a generic expression can be better proposed to cover all cases of practical interest in spudcan penetration on clay.

4.5 Conclusion

This chapter shows the application of Press-Replace (PR) Technique for spudcan penetration in single layer soil. Although there is a limitation to capture a proper flow mechanism in deep penetration. The PR Technique can be used as an alternative method to obtain load penetration curves. Some important conclusions are outlined, as follows:

- There is a required boundary distance in using PR Technique. The lateral and bottom boundary should be placed a certain distance away so that they do not affect the load penetration response. It is found that the boundary distance in non-dilative sand is greater than that in clay, *BD*= 4*B* and *BD*= 3*B* accordingly.
- There is no notable difference in applying various interface properties (R_{inter}). The R_{inter} is therefore set to be 0.7 as recommended in the PLAXIS manual.
- Changing the Young modulus in clay has no prominent effect, while having a higher Young modulus in sand will give a higher penetration resistance.
- The *stress-level-effect* can be observed for spudcan penetration in sand. N_γ decreases with increasing footing diameter, *B*. Consequently, bearing capacity factor, N_γ, can be found for different footing sizes on loose and medium dense sand.

- Dilatancy angle has a great influence on the load penetration response, and it also affects the bearing capacity factors. Hence, a proper value of dilatancy angle should be used for spudcan penetration assessments.
- Soil backflow cannot be captured in the present study. This might lead to the inaccuracy for spudcan penetration into clay. Large deformation finite element analysis would be required to fully capture the flow mechanism in the continuous spudcan penetration and better predict the load penetration response.
- The design charts presented in this chapter might only be valid for the parameters used in the present study. More validation is needed to provide more generic expression in spudcan penetration assessment.

Chapter 5.
Penetration in Double Layered System

In practice, layered system is commonly encountered and the installation process can be hazardous, with the potential of punch-through failure when spudcan penetrates into strong over weak materials. This chapter investigates the load penetration curves of spudcan penetrating on sand overlying clay. Firstly, comparison with existing experiment and numerical simulation is presented. A parametric study is then carried out to see the effect of the main input parameters, such as the sand thickness on the upper layer, the friction angle of the sand layer, and the undrained shear strength of the underlying clay. The parametric study focuses on spudcan penetrating on loose sand overlying clay.

5.1 Comparison

One case is simulated according to the numerical analysis presented by Hu et al. (2014). Spudcan with 6m of diameter penetrates into medium dense sand overlying clay. The sand thickness equals to the spudcan diameter, H_s/B= 1. The sand stiffness is assumed to be constant since there is no detailed information can be obtained. The simulation is performed by keeping the bottom boundary at 10*B* from the domain surface. The lateral domain boundary is also kept at a distance of 10*B* from the center of the spudcan. Table 5-1 shows all the prescribed parameters for this case.

Table 5-1 Parameters of centrifuge and numerical test of medium dense sand overlying clay from Hu et al. (2014).

Test Name	Geometry		Sand				Clay				
	H_s	B	E	γ'_s	φ	ν	E/s_{um}	s_{um}	k	γ'_c	ν
	[m]	[m]	[MPa]	[kN/m^3]	[^{0}]	[-]	[-]	[kPa]	[kPa/m]	[kN/m^3]	[-]
L1SP1	6	6	25	9.96	31	0.3	500	12.96	1.54	6	0.495

The result from PR Technique, CEL and experiment test by Hu et al. (2014) are presented in Figure 5-1.

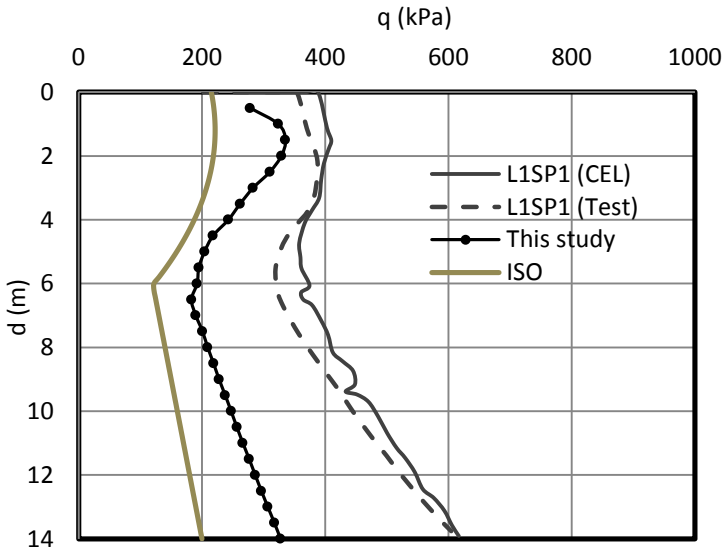

Figure 5-1 Comparison to other solutions from Hu et al. (2014).

It is expected that the result from PR Technique lies between the ISO approach and large deformation analysis such as CEL or experiment test. In addition, punching shear method provided by ISO 19905-1: 2012 is used to calculate the penetration response in Figure 5-1. Cassidy et al. (2015) mentioned two possible reasons that lead to the underestimation of load penetration response when the approach by ISO is used: (1) The method is originally developed for shallow wished-in-place footings, and not for continuous penetration like spudcan foundations and (2) the method is for stress magnitudes significantly lower than those experienced by spudcan.

In contrast to the CEL and experiment test, the trapped underneath the spudcan cannot be modelled, see Figure 2-9 for the schematic diagram. As discussed in subchapter 2.4, the shape and thickness of the sand plug might change as some sand escapes and flows around the foundation during the penetration process. The sand plug can grow with a height up to $0.9H_s$ and will have a great influence in the penetration response (Hu et al., 2014). The limitation of the PR Technique to model this trapped sand might explain why the present study underestimates the bearing pressure compared to the CEL approach and experiment test.

5.2 Parametric study

Many studies have been done for dense or very dense sand overlying clay. Hence, parametric study is carried out and focused on penetration in loose sand overlying clay, using an alternative method, PR Technique. The effect of the sand thickness, the friction angle of the sand layer, and the undrained shear strength of the underlying clay will be discussed.

The influence of dilatancy angle is not taken into account in this parametric study since it is commonly known that dilatancy angle does not play a role in loose sand. Furthermore, the boundary distance is kept at a distance of 10*B* from the reference axis in all analyses. The investigated cases in this section are listed below:

a. *Spudcan geometry:* B = 5, 10, 15 m.
b. *Effective unit weight:* γ'_s = 8 kN/m^3 and γ'_c= 6 kN/m^3.
c. *Friction angle*: φ= 25^0, 27^o, 29^o.
d. *Undrained shear strength at the interface:* s_{um}= 10 – 45 kPa.
e. *Degree of non-homogeneity:* kB/s_{um}= 0.5 and 1.

All the cases are also tabulated in Appendix B.

5.2.1 Influence of the undrained shear strength of the underlying clay.

In order to see the effect of the undrained shear strength of the bottom clay, some cases are picked and presented in Figure 5-2 and Table 5-2. The results of other cases can be seen in Appendix B.

Table 5-2 Some cases to investigate the effect of s_{um}.

Case	H_s [m]	B [m]	H_s/B [-]	φ [^{o}]	s_{um} [kPa]	k [kPa/m]	kB/s_{um} [-]
SC13a	2.5	5	0.5	27	7.5	1.5	1
SC13	2.5	5	0.5	27	10	2	1
SC31a	5	10	0.5	27	15	1.5	1
SC31	5	10	0.5	27	20	2	1
SC49a	7.5	15	0.5	27	22.5	1.5	1
SC49	7.5	15	0.5	27	30	2	1
SC14a	3.75	5	0.75	27	7.5	1.5	1

SC14	3.75	5	0.75	27	10	2	1
SC32a	7.5	10	0.75	27	15	1.5	1
SC32	7.5	10	0.75	27	20	2	1
SC50a	11.25	15	0.75	27	22.5	1.5	1
SC50a	11.25	15	0.75	27	30	2	1

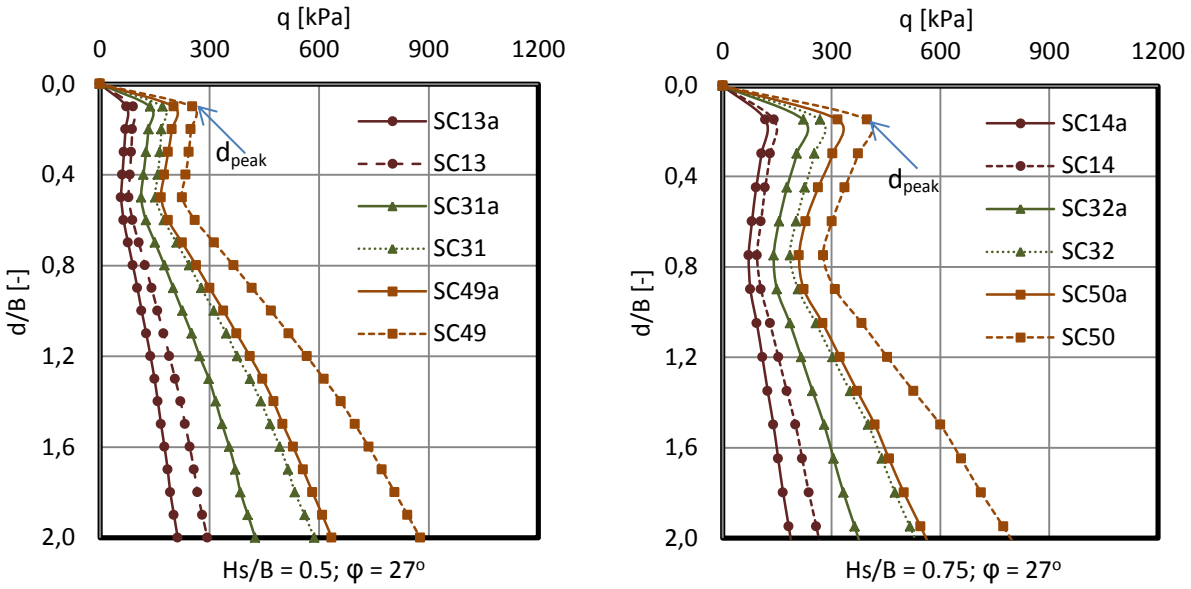

Figure 5-2 Effect of the undrained shear strength of the bottom clay on the penetration response.

Figure 5-2 shows that the bearing resistance increases with increasing undrained shear strength and spudcan diameter. Changing the undrained shear strength only modify the magnitude of the penetration response, however the occurrence of punch-through is mainly determined by the geometry ratio H_s/B. It is also observed that the depth of the peak penetration resistance, d_{peak}, from the mudline is independent of the undrained shear strength of the underlying clay.

5.2.2 Influence of the sand thickness and the friction angle of upper sand layer.

As mentioned previously, the punch-through possibility depends on the geometry ratio, H_s/B. This influence of the sand thickness will be discussed in this section and only some cases are presented. The other results can be seen in Appendix B. Figure 5-3 and Figure 5-4 show the influence of the sand thickness and the friction angle of the upper sand layer. The bearing pressure is also presented as a dimensionless pressure by having a normalization with respect to the undrained shear strength of the clay at the interface between sand and clay, s_{um}. Having this normalization will help in interpreting the load penetration curves.

In general, punch-through is more likely to happen for higher H_s/B. There is an obvious reduction of the peak resistance in the upper layer compared to the case for thinner sand layer (small H_s/B). Higher H_s/B will also give a higher peak resistance. It is reasonable to explain that the contribution of the sand on the peak resistance would be more for the thickest sand layer.

For small sand thickness ratio, H_s/B= 0.5, the resistance in the upper layer is approximately constant, no obvious peak value can be seen. This is often called rapid-leg-run event in the jack-up industry. Both punch-through and rapid-leg-run event might lead to the uncontrolled leg penetration of the jack-up units. Similar findings on the influence of the sand thickness are also found by Teh (2007), Lee (2009), and Hu et al. (2014) in the case of medium dense or dense sand overlying clay.

Hu et al. (2014) further explained that, for larger H_s/B, the sand bearing capacity provides the majority of the peak resistance, q_{peak}. In contrast, the contribution of the clay bearing capacity might dominate for small H_s/B. The clay bearing capacity mainly depends on the undrained shear strength, s_{um}, and the increase of the strength over the depth, k, which do not change when the analysed on the influence of sand thickness ratio are conducted; as a consequence, the severity of punch-through is more likely to occur with a larger sand thickness ratio, H_s/B.

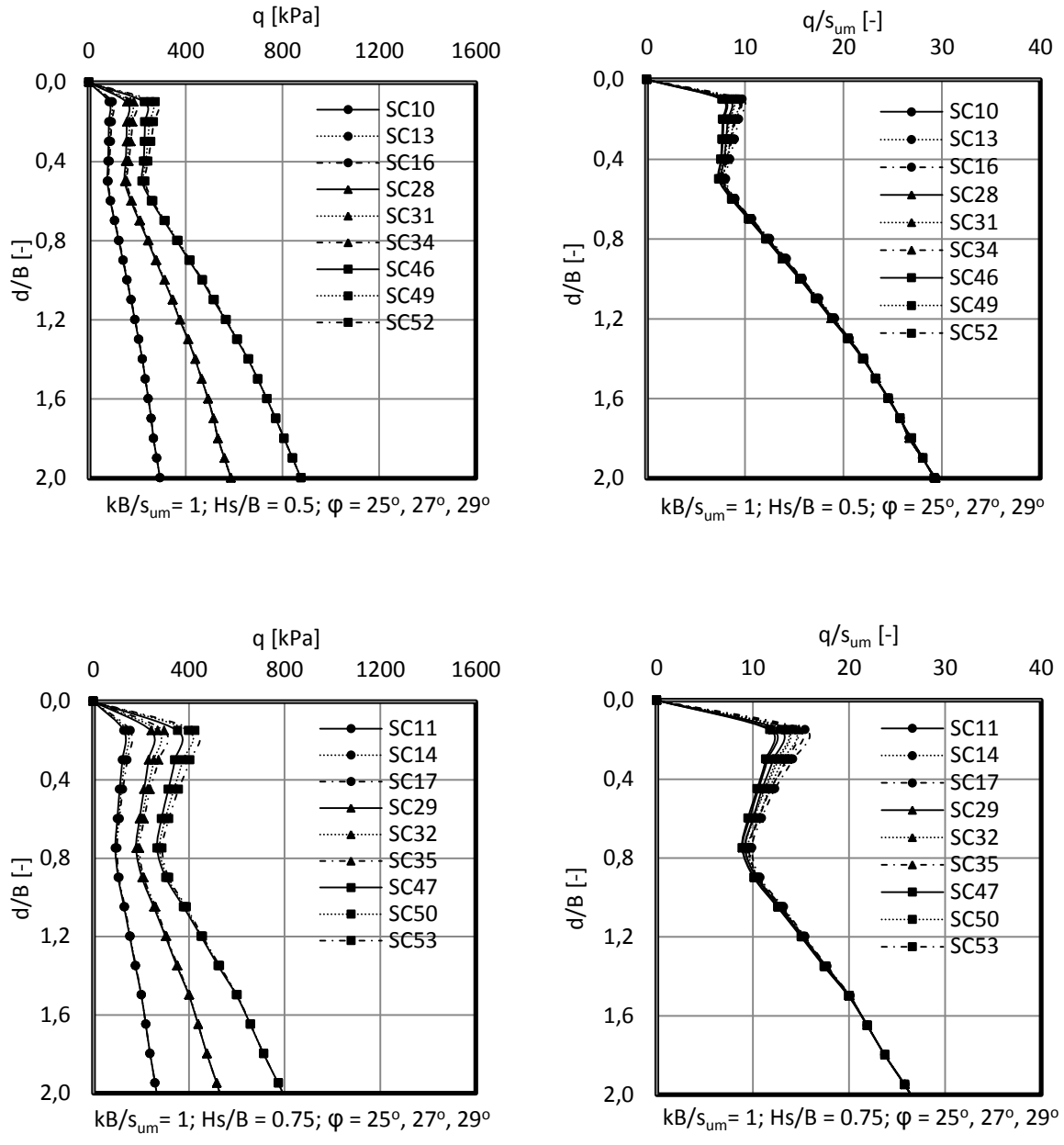

Figure 5-3 The influence of sand thickness (H_s/B = 0.5 & 0.75) and the friction angle.

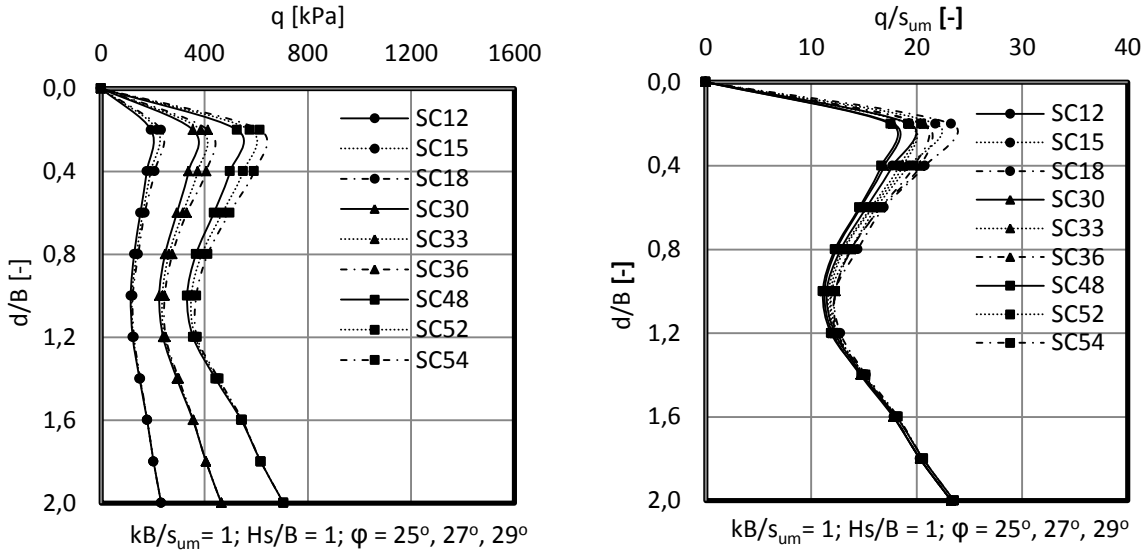

Figure 5-4 The influence of sand thickness (H_s/B = 1) and the friction angle.

Different values of a friction angle are also set in Figure 5-3 and Figure 5-4. The figures show that having a higher friction angle will lead to an increase in the peak bearing pressure, yet the resistance in the second layer remains the same. The existence of punch-through or rapid-leg-run event is independent of the friction angle of the sand layer. These trends also imply that the design charts should be constructed based on the ratio of H_s/B.

Furthermore, Figure 5-5 shows the soil deformation patterns from PLAXIS. SC28, SC29, and SC30 are conducted with the same soil condition: φ= 25°, γ'_s= 8 kN/m^3, γ'_c= 6 kN/m^3. The same footing size diameter is used, B= 10m. The sand thickness ratio is varied, H_s/B= 0.5, 0.75, and 1, for SC28, SC29, SC30 respectively. Figure 5-5 clearly depicts that the soil flow takes place in the sand and clay layer. This suggests that the failure mechanism involves the strength mobilization of both soil layer. As previously discussed in subchapter 2.4, the failure mechanism that involve both layers results in the reduction on the penetration resistance because of the strength contrast between the upper and lower layer.

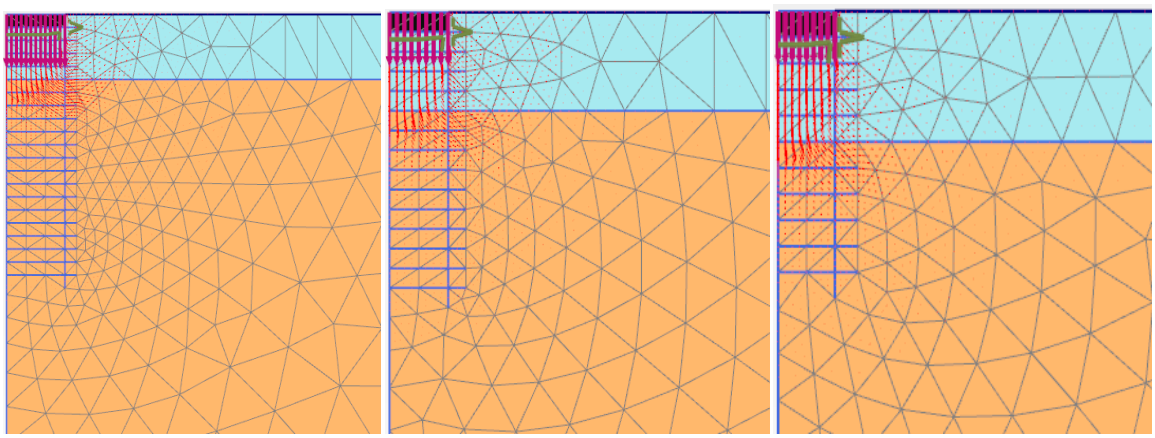

Figure 5-5 Soil deformation pattern for various H_s/B, Case: SC28, SC29, and SC30.

5.3 Peak resistance and depth of peak resistance

Based on the parametric study, an attempt is made to produce design charts. As previously described in subchapter 2.4, the penetration resistance profile in double layered system is commonly divided into two phases: (1) the resistance in the upper layer, q_{peak} and (2) the resistance in the clay layer, q_{clay}. This section discusses the resistance in the upper layer.

Firstly, the peak resistance calculated from PR Technique is compared to the solution provided by ISO, using punching shear method. The diagonal line (blue line) in Figure 5-6 is the equality line. Figure 5-6 shows that the punching shear method underestimates the q_{peak} values based on The PR-Technique. The solution from ISO tends to be more conservative with a thick sand layer, e.g. H_s/B= 1. The reason of the underestimation might be explained by looking at the schematic diagram, Figure 5-7, which is based on the soil deformation pattern from the visualisation experiment conducted by Teh (2007). Compared to the punching shear method (the schematic diagram can be seen in Figure 2-8(b)), the actual slip surface is curved and inclined outward. As a result, the soil is mobilized over a larger projected area than the spudcan size.

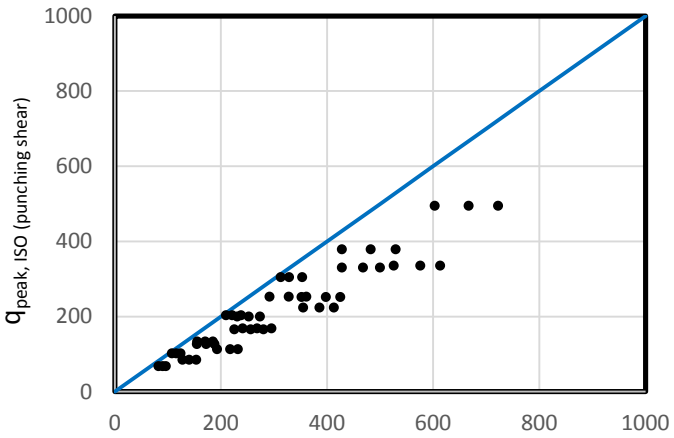

Figure 5-6 Comparison between PR Technique and punching shear method.

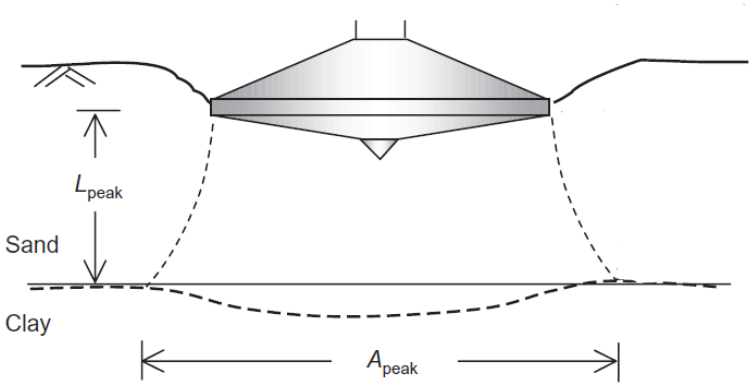

Figure 5-7 Schematic diagram of failure mechanism observed during q_{peak} (Teh, et al., 2008).

Secondly, the depth of the peak resistance is approximated based on the parametric study. The d_{peak} is plotted against the sand thickness ratio, H_s/B, in Figure 5-8 that leads to the following expression:

$$d_{peak} = 0.2\, H_s\,;\; 0.5 \leq \frac{H_s}{B} \leq 1 \tag{5-1}$$

This shows that the peak resistance occurs at a relatively shallow embedment, which is in line with findings by other researchers (see subchapter 2.4).

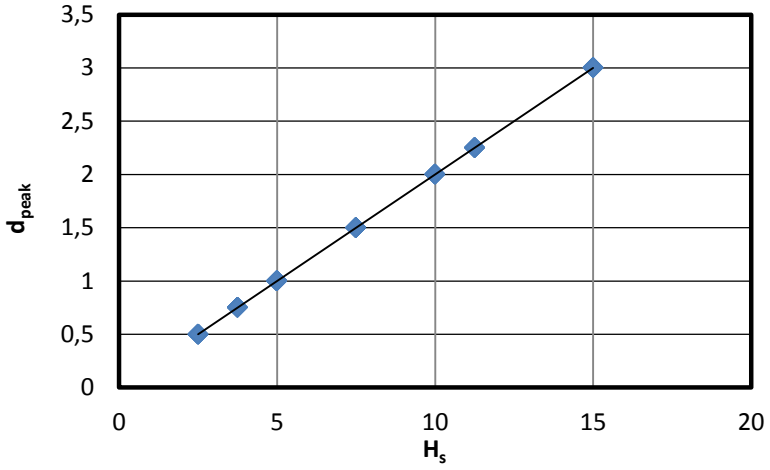

Figure 5-8 Approximate curve for the depth of the peak resistance.

Lastly, following the normalization done by Lee (2009), Figure 5-6 is replotted and the normalized peak resistance is presented against H_s/B in Figure 5-9. It is also observed here that the peak resistance increases with the increase of sand thickness and friction angle of the upper sand layer.

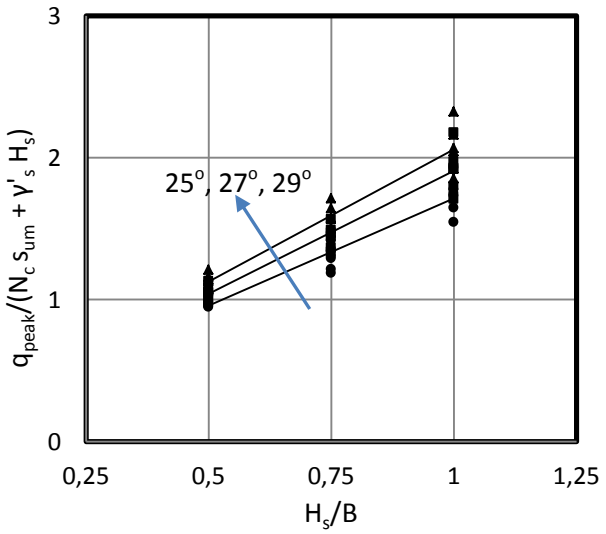

Figure 5-9 Normalized peak resistance for the investigated case.

5.4 Penetration resistance in the underlying clay

Based on the parametric study, the resistance in the underlying clay mainly depends on the shear strength and the increase rate of the undrained shear strength. The resistance in the underlying clay is assessed separately in this section. Using equation 2-1, the bearing capacity factors, N_c, can be back calculated from all the investigated cases in the present study. In Figure 5-10, the N_c values are then plotted against a new parameter that represents the strength ratio of sand to clay (R_{sc}) which is proposed by Yu et al. (2012).

$$R_{sc} = \frac{H_s \, \gamma'_s \tan \varphi}{s_{um}} \tag{5-2}$$

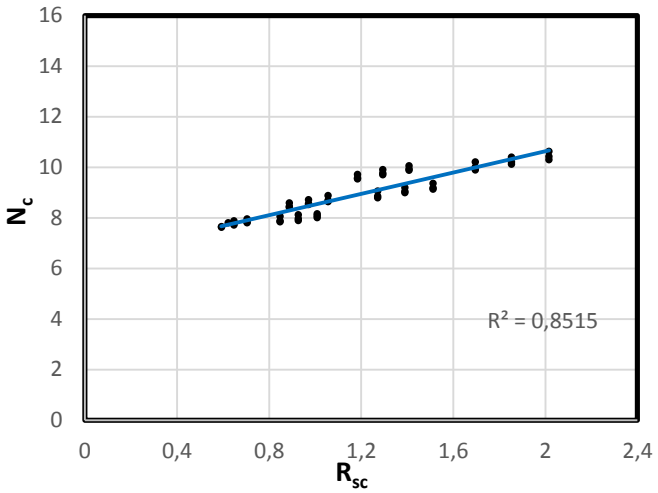

Figure 5-10 N_c vs R_{sc}.

A linear trend is found and the following expression can be proposed to calculate penetration resistance in the underlying clay:

$$N_c = 2.1006 \, R_{sc} + 6.4316 \tag{5-3}$$

$$q_{clay} = (2.1006 \, R_{sc} + 6.4316) s_u + \gamma'_c \, d \tag{5-4}$$

It should be noted that all the proposed charts or expressions presented in this chapter might only be valid for the investigated cases in the present study. More parametric study might be needed so that a generic expression can be better proposed to cover all cases of practical interest in spudcan penetration on sand overlying clay.

5.5 Conclusion

This chapter shows the application of Press-Replace (PR) Technique for spudcan penetration in double layered soil deposits, loose sand overlying clay. PR Technique shows its capability to be an alternative method to obtain load penetration curves. Some important conclusions are outlined, as follows:

- This study proves that a potential punch-through failure can still be found in spudcan penetrating into loose sand overlying clay.
- For a spudcan penetrating on a thin sand overlying clay (H_s/B= 0.5), there is no obvious peak value in the upper sand layer. The peak resistance is approximately constant. On the other hand, the punch-through potential is more likely to occur with a thick sand layer (H_s/B= 1).
- The occurrence of punch-through or rapid-leg-run event is mainly dependent on the geometry aspect, which is the sand thickness ratio, H_s/B.
- The depth of the peak penetration resistance, d_{peak}, is also dependent on the sand thickness ratio H_s/B. Having a larger friction angle in the upper layer will only increase the peak resistance without changing the location of d_{peak}.
- Changing the undrained shear strength only modifies the magnitude of the penetration response especially for the penetration resistance in the second layer. However, the onset of punch-through is mainly determined by the geometry ratio H_s/B.
- The design charts presented in this chapter might only be valid for the parameters used in the present study. More validation is needed to provide more generic expression in spudcan penetration assessment.

Chapter 6.
Conclusion and Further Research

6.1 Conclusion

The present study is focused on the investigation of spudcan penetration into single layer system (sand and clay) and double layered soil deposits, sand overlying clay. Finite element analysis, using PLAXIS 2D 2015, is used to study the penetration of spudcan foundations subjected to vertical loading. All simulations are carried out with a 2D axisymmetric model and Mohr-Coulomb constitutive soil model. The major achievement of this research is the application of The Press-Replace (PR) Technique to simulate spudcan penetration in homogeneous and two layered soil deposits.

The results from this technique are initially compared against experimental tests and also other solutions from large deformation finite element analyses. Parametric study is also undertaken to see the influence of the main input parameters on the load penetration curves. The main findings are summarized below.

6.1.1 Spudcan penetration in single layer

The finite element analysis in Chapter 4 showed evidence of (i) the effect of boundary distance; (ii) the influence of the Young modulus for spudcan penetration in sand; (iii) the *stress-level-effect* in which the bigger spudcan gives lower bearing capacity factors; (iv) the prominent influence of dilatancy angle on the penetration response; and (v) deep bearing capacity factors for penetration in clay.

Some checks are initially carried out to observe whether the PR-Technique used in this study is free from boundary distance effect, to see the influence of the slice thickness or the step size of the prescribed displacement, and to investigate the effect of the Young modulus as one of the main input parameters. These checks form a basis for undertaking the parametric study.

In general, having a bigger footing size, a higher friction angle, or a higher undrained shear strength will give a higher penetration resistance. The penetration curves are also presented in dimensionless forms, giving a better insight on how some parameters influence the load penetration curves. For penetration in sand layer, the bearing capacity factor, N_γ, is dependent on the footing size. The smaller the spudcan is, the larger the bearing capacity factor is. It is also revealed that the dilatancy angle has a great influence on the N_γ, therefore it gives a significant effect on the penetration resistance. Although obtaining the exact value of N_γ is not the objective of the present study, the findings of this study show that a proper value of dilatancy angle should be used, especially when using finite element program, to assess spudcan penetration process.

The change of soil flow mechanism can still be observed. This change might also explain the alteration of the slope of the load penetration curves, especially for spudcan penetration in clay. It is observed that for shallow embedment, the soil flow occurs with some surface movement. However, the flow mechanism becomes more localized as the spudcan penetrates deeper.

The bearing capacity factor for penetration in clay, N_c, increases gradually at shallow penetration and have the attainment of limiting bearing capacity factor, N_{cd}, at around penetration depth of d/B=

1.1 – 1.2. This bearing capacity factor becomes independent of the normalized strength, $s_{um}/\gamma' B$, and the degree of non-homogeneity, kb/s_{um}, in deep penetration. It should be highlighted that the cavity above spudcan is preserved in all simulations for spudcan penetration in clay. Design charts are also presented, however they might only be valid for the parameters used in the present study.

6.1.2 Spudcan penetration in double layered system

The finite element analysis in Chapter 5 focuses on the bearing response of spudcan foundations on sand overlying clay. Previous studies were mainly focused on the punch-through potential for spudcan penetration in dense or very dense sand overlying clay. The present study proves that punch-through can also occur when spudcan penetrates into loose sand overlying clay. The significant reduction of the peak resistance can be observed in this study, that refers to punch-through potential. Parametric study is also carried out by varying the sand thickness ratio, the spudcan diameters, the friction angle, and also the undrained shear strength of the underlying clay soil in order to see the influence of these main parameters on the load penetration curves.

Based on the parametric study, the onset of the punch-through or rapid-leg-run event is mainly determined by the sand thickness ratio, H_s/B. The punch-through potential is more likely to occur with a thick sand layer (H_s/B= 1), while rapid-leg-run event happens with a thin sand overlying clay. In addition, the depth of peak penetration resistance, d_{peak}, is also dependent on the sand thickness ratio, H_s/B. The friction angle of the upper sand layer will just modify the peak penetration resistance without changing the resistance in the underlying clay layer since the resistance for the second layer is mainly governed by the undrained shear strength of the clay deposit, s_u.

The solution from PR technique is also checked against the approach recommended by the industry guideline, ISO 19905-1: 2012. The solution from this study overestimates the penetration resistance compared to the punching shear method provided by ISO. This might be because the punching shear method was originally developed for a wished-in-place shallow foundation. Furthermore, an attempt to normalize the bearing pressure and some design charts are also presented, however they might only be valid for the parameters used in the present study.

6.1.3 The limitation of Press-Replace (PR) Technique

The PR Technique employed in this study shows its capability to be an alternative method to produce and investigate the load penetration curves of spudcan foundations of offshore jack-up rigs. In addition, the PR Technique can qualitatively predict the occurrence of possible punch-through failure. This technique can be used in any commercial geotechnical software, such as PLAXIS. Although large deformation numerical analysis would be required in order to correctly model continuous penetration, PR Technique can still provide reliable full penetration profiles for spudcan penetration into homogeneous and two layered soil deposits. Some limitations should be noted that might explain why the result from PR Technique is different to other experimental tests and large deformation finite element analysis.

- The method is not able to capture backflow mechanism, especially for penetration in clay.
- Sand plug plays an important role for penetration in sand overlying clay. The trapped sand underneath the spudcan is not modelled in this study. This might explain why the solution from PR Technique underestimates the resistance compared to other solution from experimental tests or large deformation finite element analysis.

6.2 Recommendation for future research

The following is recommended to improve the understanding of spudcan penetration assessment, using PR Technique:

- All simulations in the present study are using Mohr-Coulomb as a constitutive model. It would be interesting to see the load penetration response applying different soil constitutive models. One of the important aspects that can be investigated further using more advanced soil constitutive model is the influence of dilatancy in the penetration response. As discussed in subchapter 4.4.1.2, the end of dilatancy, as generally observed when the soil reaches the critical state cannot be modelled using the Mohr-Coulomb constitutive soil model. For future work, Hardening Soil model might be an alternative option to examine the influence of dilatancy using *Dilatancy Cut-Off* in modelling the end of diltancy.
- In order to develop more generic design charts, further investigation or parametric study is required, by varying soil properties and spudcan geometry that are in practical interests.
- For future research, apart from using experimental tests, it is suggested to verify the results from PR Technique against the field data (actual penetration data).
- The framework of the current research might be extended to investigate spudcan penetration into multi-layered soils (more than two layered soil deposits) based on the fact that more stratified soils can be found in many offshore areas.
- This research is only limited to a spudcan under vertical loading condition. Other site specific assessments such as a yield interaction and sliding check might be included for future research.

References

Andersen, K. H., Andresen, L., Jostad, H. P., & Clukey, E. C. (2004). Effect of skirt-tip geometry on set-up outside suction anchors in soft clay. *Proc. 23rd Int. Conf. on Offshore Mechanics and Arctic Engineering*, *1*, pp. 1035–1044. Vancouver.

Bienen, B., Qiu, G., & Pucker, T. (2015). CPT correlation developed from numerical analysis to predict jack-up foundation penetration into sand overlying clay. *Ocean Engineering*, 216-226.

Bolton, M. D. (1986). Strength and dilatancy of sands. *Geotechnique, 36(1)*, 65-78.

Bolton, M. D., & Lau, C. K. (1993). Vertical bearing capacity factors for circular and strip footings on Mohr-Coulomb soil. *Canadian Geotechnical Journal 30, no. 6*, 1024-1033.

Bowles, J. E. (1997). *Foundation Analysis and Design.* Singapore: The McGraw-Hill Companies, Inc.

Brinkgreve, R. B., Engin, E., & Engin, H. K. (2010). Validation of empirical formulas to derive model parameters for sands. *7th NUMGE.* Trondheim, Norway. doi:10.1201/b10551-25

Brinkgreve, R. B., Kumarswamy, S., & Swolfs, W. M. (2015). *PLAXIS 2D.* Delft.

Budhu, M. (2011). *Soil Mechanics and Foundations* (3rd ed.). Hoboken: John Wiley & Sons, Inc.

Cassidy, M. J., & Houlsby, G. T. (1999). On the modelling of foundations for jack-up units on sand. *In Offshore Technology Conference. Offshore Technology Conference*.

Cassidy, M. J., & Houlsby, G. T. (2002). Vertical bearing capacity factors for conical footings on sand. *Géotechnique 522002*, No.9, 687-692.

Cassidy, M., Li, J., Hu, P., Uzielli, M., & Lacasse, S. (2015). Deterministic and probabilistic advances in the analysis of spudcan behaviour. In V. Meyer (Ed.), *The Third International Symposium on Frontiers in Offshore Geotechnics (ISFOG 2015)* (pp. 183-211). Oslo, Norway: CRC Press.

Chen, W. F. (2008). *Limit Analysis and Soil Plasticity.* J. Ross Publishing.

Chen, W., & Saleeb, A. (1983). *Constitutive equations for engineering materials.* United States: John Wiley & Sons, Inc.

Craig, W. H., & Chua, K. (1990). Deep penetration of spudcan foundation on sand and clay. . *Gèotechnique 10(4)*, 541–556.

Das, B. M. (2010). *Principles of Geotechnical Engineering* (7th ed.). Stamford: Cengage Learning.

Dean, E. R. (2008). Consistent preload calculations for jackup spudcan penetration in clays. *Canadian geotechnical Journal 45, No.5*, 705-714.

Dean, E. R. (2010). *Offshore geotechnical engineering.* London: Thomas Telford Limited.

Drescher, A., & Detournay, E. (1993). Limit load in translational failure mechanisms for associative and non-associative materials. *Geotechnique*, No. 3, 443-456.

Edwards, D., Zdravkovic, L., & Potts, D. M. (2005). Depth factors for undrained bearing capacity. *Géotechnique 55, No. 10*, 755-758.

Engin, H. K. (2013). *Modelling of pile installation effects – a numerical approach.* Ph. D. thesis, Delft University of Technology, Delft.

Engin, H. K., Brinkgreve, R. B., & van Tol, F. (2015). Simplified numerical modelling of pile penetration – the press-replace technique. *Int. J. for Num. and Analytical Meth. in Geomech*.

Engin, H. K., Khoa, H., Jostad, H. P., & Alm, T. (2015). Finite element analyses of spudcan – subsea template interaction during jack-up rig installation.

Erickson, H. L., & Drescher, A. (2002). Bearing capacity of circular footings. *Journal of Geotechnical and Geoenvironmental Engineering*, 38-43.

Fellenius, B. H. (2016). *Basics of Foundation Design.* Sidney, British Columbia.

Hanna, A. M., & Meyerhof , G. G. (1980). Design charts for ultimate bearing capacity of foundations on sand overlaying soft clay. *Canadian Geotechnical Journal*, 1: 300 - 303.

Hansen, B. (1970). *A revised and extended formula for bearing, Bulletin No.28*, 5-11. Copenhagen, Denmark: Danish Geotechnical Inst.

Hill, R. (1950). *The mathematical theory of plasticity.* London: Oxford University Press.

Hossain, M. S. (2008). *New Mechanism-Based Design Approaches for Spudcan Foundations on Clays.* Ph. D. thesis, The University of Western Australia.

Hossain, M. S., & Randolph, M. F. (2009). New mechanism-based design approach for spudcan foundations on single layer clay. *Journal of Geotechnical and Geoenvironmental Engineering*, 135(9), 1264-1274.

Hossain, M. S., & Randolph, M. F. (2009). SS: Jack-up rig technology - new mechanism- based design approach for spudcan foundations on stiff-over-soft clay. *In Offshore Technology Conference. Offshore Technology Conference*.

Hossain, M. S., Hu, Y., & Randolph, M. F. (2003). Spudcan foundation penetration into uniform clay. Honolulu, Hawaii, USA: Proceedings of The Thirteenth International Offshore and Polar Engineering Conference.

Hossain, M. S., Randolph, M. F., Hu, Y., & White, D. J. (2006). Cavity stability and bearing capacity of spudcan foundations on clay. *Proc. Offshore Technology Conference.* Houston, OTC 17770.

Houlsby, G. T., & Martin, C. (2003). Undrained bearing capacity factors for concical footings on clay. *Géotechnique*, 53(5): 513-520.

Hu, P., Wang, D., Cassidy, M. J., & Stanier, S. A. (2014). Predicting the resistance profile of a spudcan penetrating sand overlying clay. *Canadian Geotechnical Journal*, 51: 1151–1164.

Hu, P., Wang, D., Stanier, S. A., & Cassidy, M. J. (2015). Assessing the punch-through hazard of a spudcan on sand overlying clay. *Géotechnique 65, No. 11*, 883-896.

InSafeJIP. (2011). *Improved Guidelines for The Prediction of Geotechnical Performance of Spudcan Foundations During Installation and Removal of Jack-Up Units.*

ISO 19905-1. (2012). International Organization for Standardization.

Lee, K. (2009). *Investigation of potential spudcan punch-through failure on sand overlying clay soils.* The University of Western Australia.

Lee, K. K., Cassidy, M. J., & Randolph, M. F. (2013). Bearing capacity on sand overlying clay soils: experimental and finite element investigation of potential punch-through failure. *Géotechnique 63, No. 15,*, 1271-1284.

Loukidis, D., & Salgado, R. (2009). Bearing capacity of strip and circular footings in sand using finite elements. *Computers and Geotechnics 36*, 871-879.

Martin, C. M. (2003). User guide for ABC - Analysis of Bearing Capacity. *(OUEL 2261/03)*. Department of Engineering Science, University of Oxford. Retrieved from http://www-civil.eng.ox.ac.uk/people/cmm/software/abc/

Menzies, D., & Roper, R. (2008). Comparison of Jackup Rig Spudcan Penetration Methods in Clay. *Proc. Offshore Technology Conference.* Houston.

Meyerhof, G. (1963). Some recent research on bearing capacity of foundations. *Canadian Geotechnique Journal*, 1(1): 16 - 26.

Potts, D., & Zdravkovic, L. (1999). *Finite element analysis in geotechnical engineering, Theory.* London: Thomas Telford Ltd.

Potts, D., & Zdravkovic, L. (2001). *Finite element analysis in geotechnical engineering, Application.* London: Thomas Telford Ltd.

Prandtl, L. (1921). Eindringungsfestigkeit und festigkeit von schneiden. *Z. Angew. Math. Mech.*, 1, 15.

Pucker, T., Bienen, B., & Henke, S. (2012). Numerical simulation of spudcan penetration into silica sand and prediction of bearing behaviour. *Proceedings of 31st International Conference on Ocean, Offshore, and Arctic Engineering.* Rio de Janeiro. doi:10.1115/OMAE2012-83042

Qiu, G., Henke, S., & Grabe, J. (2010). 3D FE analysis of the installation process of spudcan foundations. *2nd International Symposium on Frontiers in Offshore Geotechnics, ISFOG*, (pp. 685-690). Perth WA.

Randolph, M., & Gourvenec, S. (2011). *Offshore Geotechnical Engineering.* Spon Press.

Rigzone. (2016). Retrieved from http://www.rigzone.com/

Royal IHC. (2016). Retrieved from http://www.royalihc.com/

Salgado, R., Lyamin, A. L., Sloan, S. W., & Yu, H. (2004). Two and three-dimensional bearing capacity of foundations in clay. *Géotechnique*, 54(5): 297-306.

Sivasithamparam, N., Engin, H. K., & Castro, J. (2015). Numerical modelling of pile jacking in a soft clay. *Computer Methods and Recent Advances in Geomechanics.* Kyoto, Japan.

Skempton, A. W. (1951). The bearing capacity of clays. *Proc., Building Research Congress*, *1*, pp. 180-189. London.

Sloan, S. W., & Randolph, M. F. (1982). Numerical prediction of collapse loads using finite element methods. *International JOurnal for Numerical and Analytical Methods in Geomechanics*, 6(1): 47 - 76.

Society of Naval Architects (SNAME). (2002). *Recommended practice for site specific assessment of mobile jack-up units* (T&R Bulletin 5-5A, 1st Ed. - Rev.2 ed.). N.J.

Teh, K. L. (2007). *Punch-through of spudcan foundation in sand overlying clay.* National University of Singapore, Civil Engineering.

Teh, K. L., Cassidy, M., Leung, C. F., Chow, K. Y., Randolph, M., & Quah, C. K. (2008). Revealing the bearing capacity mechanisms of a penetrating spudcan through sand overlying clay. *Géotechnique*, 58(10): 793-804.

Teh, K. L., Leung, C. F., Chow, Y. K., & Cassidy, M. J. (2010). Centrifuge model study of spudcan penetration in sand overlying clay. *Geotechnique 60*, No.11, 825-842.

Tehrani, F. S., Nguyenb, P., Brinkgreve, R. B., & van Tol, F. (2016). Comparison of Press-Replace Method and Material Point Method for analysis of jacked piles. *Computers and Geotechnics 78*, 38-53.

Terzaghi, K. (1943). *Theoretical soil mechanics.* London: Chapman and Hall.

Ullah, S. N., Hu, Y. X., Stanier, S., & White, D. J. (2016). Lateral boundary effects in centrifuge foundation tests. *International Journal of Physical Modelling in Geotechnics*.

Ullah, S. N., Hu, Y. X., White, D. J., & Steiner, S. (2014). Lateral boundary effect in centrifuge tests for spudcan penetration in uniform clay. *Applied Mechanics and Materials, 553*, 458-463.

Ullah, S. N., Hu, Y., Stanier, S., & White, D. J. (2016). Lateral boundary effects in centrifuge foundation tests. *International Journal of Physical Modelling in Geotechnics*.

van Langen, H., & Vermeer, P. (1991). Interface elements for singular plasticity points. *Int. J. for Num. and Analytical Methods in Geomechanics*, 15, pp. 301-315.

Vesic, A. S. (1975). *Bearing capacity of shallow foundations. In Foundation Engineering Handbook, ed by Winterkorn and Fang.* New York: Van Nostrand Reinhold.

White, D. J., Teh, K., Leung, C., & Chow, K. Y. (2008). A comparison of the bearing capacity of flat and conical circular foundation. *Géotechnique*, 58(10): 781 - 792.

Wood, D. M. (2004). *Geotechnical Modelling.*

Yamamoto, N., Randolph, M., & Einav, I. (2009). Numerical study of the effect of foundation size for a wide range of sands. *Journal of geotechnical and geoenvironmental engineering*.

Yin, J. H., Wang, Y. J., & Selvadurai, A. (2001). Influence of nonassociativity on the bearing capacity of a strip footing. *Journal of Geotechnical and Geoenvironmental Engineering*, 127(11): 985-989.

Yu, L., Hu, Y., & Liu, J. (2012). Spudcan penetration in loose sand over uniform clay. *Proc. of 28th Int. Conf. on Ocean, Offshore and Arctic Engineering.* Hawaii, USA.

Yu, Y., Damians, I. P., & Bathurst, R. J. (2015). Influence of choice of FLAC and PLAXIS interface models on reinforced soil-structure interactions. *Computers and Geotechnics 65*, 164-174.

Zhu, F., Clark, J. I., & Ryan, P. (2001). Scale effect of strip and circular footings resting on dense sand. *Journal of Geotechnical and Geoenvironmental Engineering*, 127(7):613-621.

Appendix

Appendix A – Spudcan penetration in single layer

Summary of all investigated cases for spudcan penetrating sand.

Non-dilative sand (ψ= 0)

Case	B [m]	γ' [kN/m^3]	φ [^{0}]	v
S1	5	11	25	0.3
S2	5	11	27	0.3
S3	5	11	29	0.3
S4	5	11	30	0.3
S5	5	11	32	0.3
S6	5	11	34	0.3
S7	10	11	25	0.3
S8	10	11	27	0.3
S9	10	11	29	0.3
S10	10	11	30	0.3
S11	10	11	32	0.3
S12	10	11	34	0.3
S13	15	11	25	0.3
S14	15	11	27	0.3
S15	15	11	29	0.3
S16	15	11	30	0.3
S17	15	11	32	0.3
S18	15	11	34	0.3

Dilative sand (ψ≠ 0)

Case	B [m]	γ ' [kN/m^3]	φ [^{0}]	Ψ [^{0}]	v
S19	5	11	30	5	0.3
S20	5	11	30	10	0.3
S21	5	11	30	15	0.3
S22	10	11	30	5	0.3
S23	10	11	30	10	0.3
S24	10	11	30	15	0.3
S25	15	11	30	5	0.3
S26	15	11	30	10	0.3
S27	15	11	30	15	0.3
S28	5	11	32	5	0.3
S29	5	11	32	10	0.3
S30	5	11	32	15	0.3
S31	10	11	32	5	0.3
S32	10	11	32	10	0.3
S33	10	11	32	15	0.3

S34	15	11	32	5	0.3
S35	15	11	32	10	0.3
S36	15	11	32	15	0.3
S37	5	11	34	5	0.3
S38	5	11	34	10	0.3
S39	5	11	34	15	0.3
S40	10	11	34	5	0.3
S41	10	11	34	10	0.3
S42	10	11	34	15	0.3
S43	15	11	34	5	0.3
S44	15	11	34	10	0.3
S45	15	11	34	15	0.3

Summary of analysis for the investigation of step size and mesh density (clay).

Case	Slice thickness/step size (u_y= t_s)	Mesh density
E4c	1 m	Coarse
E4m	1 m	Medium
E5c	1.25 m	Coarse
E5m	1.25 m	Medium
E6c	1.5 m	Coarse
E6m	1.5 m	Medium

Summary of all investigated cases for spudcan penetrating non-homogeneous clay.

Case	B [m]	γ ' [kN/m^3]	s_{um} [kPa]	s_{um} / γ'*B [-]	k [kPa/m]	kB/s_{um} [-]
C13	5	7	5	0,142	1	1
C14	10	7	10	0,142	1	1
C15	15	7	15	0,142	1	1
C16	5	8	5	0,125	1	1
C17	10	8	10	0,125	1	1
C18	15	8	15	0,125	1	1
C19	5	7	10	0,285	2	1
C20	10	7	20	0,285	2	1
C21	15	7	30	0,285	2	1
C22	5	8	10	0,25	2	1
C23	10	8	20	0,25	2	1
C24	15	8	30	0,25	2	1
C25	5	7	15	0,428	3	1
C26	10	7	30	0,428	3	1
C27	15	7	45	0,428	3	1
C28	5	8	15	0,375	3	1
C29	10	8	30	0,375	3	1
C30	15	8	45	0,375	3	1
C31	5	7	5	0,142	2	2
C32	10	7	10	0,142	2	2

C33	15	7	15	0,142	2	2
C34	5	8	5	0,125	2	2
C35	10	8	10	0,125	2	2
C36	15	8	15	0,125	2	2
C37	5	7	7,5	0,214	3	2
C38	10	7	15	0,214	3	2
C39	15	7	22,5	0,214	3	2
C40	5	8	7,5	0,187	3	2
C41	10	8	15	0,187	3	2
C42	15	8	22,5	0,187	3	2
C43	5	7	2,5	0,071	1	2
C44	10	7	5	0,071	1	2
C45	15	7	7,5	0,071	1	2
C46	5	8	2,5	0,062	1	2
C47	10	8	5	0,062	1	2
C48	15	8	7,5	0,062	1	2

Load penetration curves of spudcan penetration in homogeneous clay.

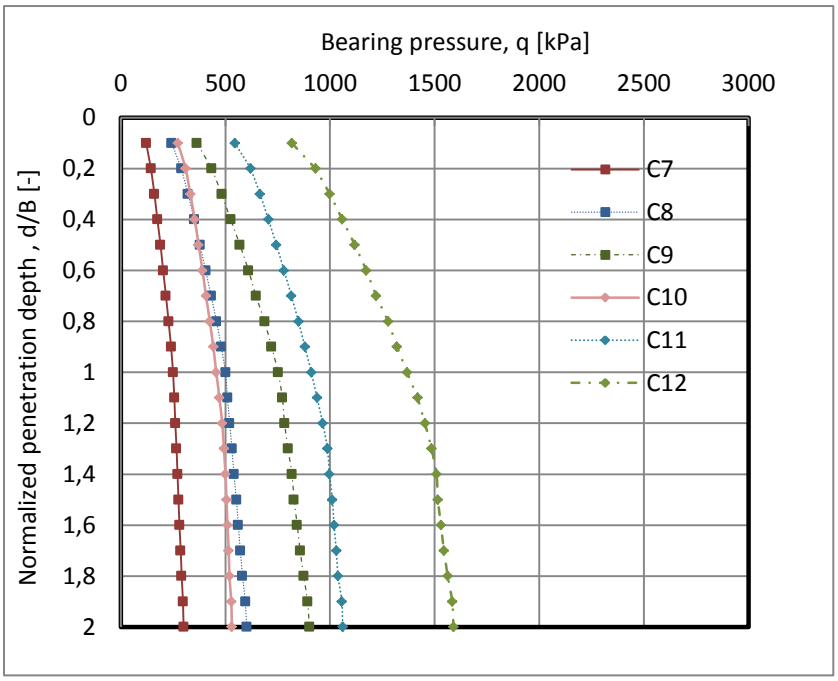

Comparison of SSFE and LDFE for spudcan penetration in clay (Hossain, 2008)

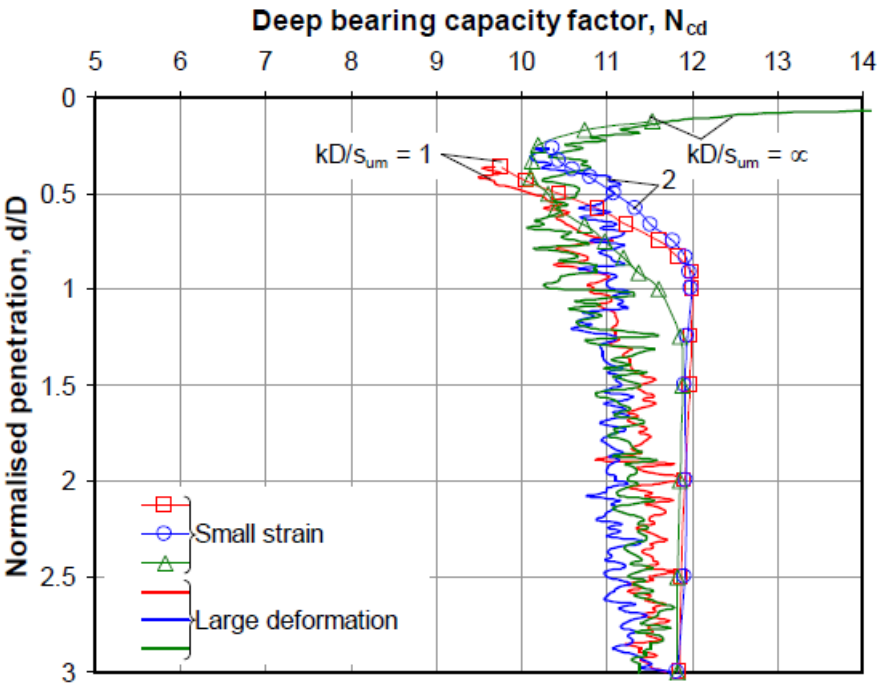

(a) Smooth-based spudcan

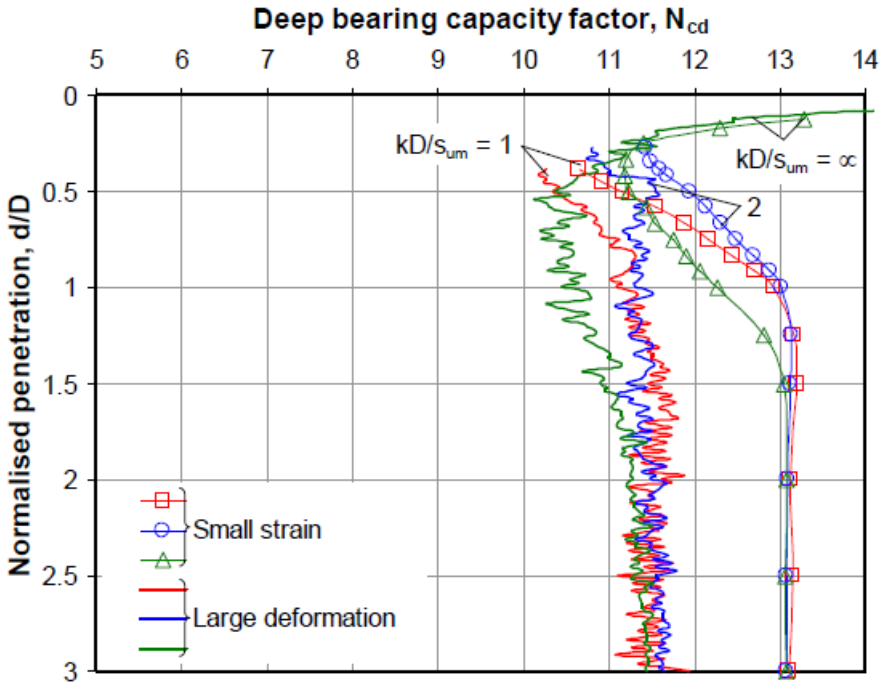

(b) Rough-based spudcan

Appendix B – Spudcan penetration in double layered system

Summary of all investigated cases for spudcan penetrating loose sand overlying clay.

Note: E_{inc}= 1000 kN/m^2/m for sand. E_{clay}= 500s_{um}. v_{sand}= 0.3 and v_{clay}= 0.495

Case	H_s	B	H_s/B	φ	tan φ	Υ'_s	Υ'_c	s_{um}	k	kB/s_{um}
	[m]	[m]	[-]	[^{0}]	[-]	[KN/m^3]	[kN/m^3]	[kPa]	[kPa/m]	[-]
SC1	2,5	5	0,5	25	0,4663	8	6	15	1,5	0,5
SC2	3,75	5	0,75	25	0,4663	8	6	15	1,5	0,5
SC3	5	5	1	25	0,4663	8	6	15	1,5	0,5
SC4	2,5	5	0,5	27	0,5095	8	6	15	1,5	0,5
SC5	3,75	5	0,75	27	0,5095	8	6	15	1,5	0,5
SC6	5	5	1	27	0,5095	8	6	15	1,5	0,5
SC7	2,5	5	0,5	29	0,5543	8	6	15	1,5	0,5
SC8	3,75	5	0,75	29	0,5543	8	6	15	1,5	0,5
SC9	5	5	1	29	0,5543	8	6	15	1,5	0,5
SC10	2,5	5	0,5	25	0,4663	8	6	10	2	1
SC11	3,75	5	0,75	25	0,4663	8	6	10	2	1
SC12	5	5	1	25	0,4663	8	6	10	2	1
SC13	2,5	5	0,5	27	0,5095	8	6	10	2	1
SC14	3,75	5	0,75	27	0,5095	8	6	10	2	1
SC15	5	5	1	27	0,50952	8	6	10	2	1
SC16	2,5	5	0,5	29	0,5543	8	6	10	2	1
SC17	3,75	5	0,75	29	0,5543	8	6	10	2	1
SC18	5	5	1	29	0,5543	8	6	10	2	1
SC19	5	10	0,5	25	0,4663	8	6	30	1,5	0,5
SC20	7,5	10	0,75	25	0,4663	8	6	30	1,5	0,5
SC21	10	10	1	25	0,4663	8	6	30	1,5	0,5
SC22	5	10	0,5	27	0,5095	8	6	30	1,5	0,5
SC23	7,5	10	0,75	27	0,5095	8	6	30	1,5	0,5
SC24	10	10	1	27	0,5095	8	6	30	1,5	0,5
SC25	5	10	0,5	29	0,5543	8	6	30	1,5	0,5
SC26	7,5	10	0,75	29	0,5543	8	6	30	1,5	0,5
SC27	10	10	1	29	0,5543	8	6	30	1,5	0,5
SC28	5	10	0,5	25	0,4663	8	6	20	2	1
SC29	7,5	10	0,75	25	0,4663	8	6	20	2	1
SC30	10	10	1	25	0,4663	8	6	20	2	1
SC31	5	10	0,5	27	0,5095	8	6	20	2	1
SC32	7,5	10	0,75	27	0,5095	8	6	20	2	1
SC33	10	10	1	27	0,5095	8	6	20	2	1
SC34	5	10	0,5	29	0,5543	8	6	20	2	1
SC35	7,5	10	0,75	29	0,5543	8	6	20	2	1
SC36	10	10	1	29	0,5543	8	6	20	2	1
SC37	7,5	15	0,5	25	0,4663	8	6	45	1,5	0,5
SC38	11,25	15	0,75	25	0,4663	8	6	45	1,5	0,5
SC39	15	15	1	25	0,4663	8	6	45	1,5	0,5

SC40	7,5	15	0,5	27	0,5095	8	6	45	1,5	0,5
SC41	11,25	15	0,75	27	0,5095	8	6	45	1,5	0,5
SC42	15	15	1	27	0,5095	8	6	45	1,5	0,5
SC43	7,5	15	0,5	29	0,5543	8	6	45	1,5	0,5
SC44	11,25	15	0,75	29	0,5543	8	6	45	1,5	0,5
SC45	15	15	1	29	0,5543	8	6	45	1,5	0,5
SC46	7,5	15	0,5	25	0,4663	8	6	30	2	1
SC47	11,25	15	0,75	25	0,4663	8	6	30	2	1
SC48	15	15	1	25	0,4663	8	6	30	2	1
SC49	7,5	15	0,5	27	0,5095	8	6	30	2	1
SC50	11,25	15	0,75	27	0,5095	8	6	30	2	1
SC51	15	15	1	27	0,5095	8	6	30	2	1
SC52	7,5	15	0,5	29	0,5543	8	6	30	2	1
SC53	11,25	15	0,75	29	0,5543	8	6	30	2	1
SC54	15	15	1	29	0,5543	8	6	30	2	1

The effect of the undrained shear strength of the underlying clay on the penetration response.

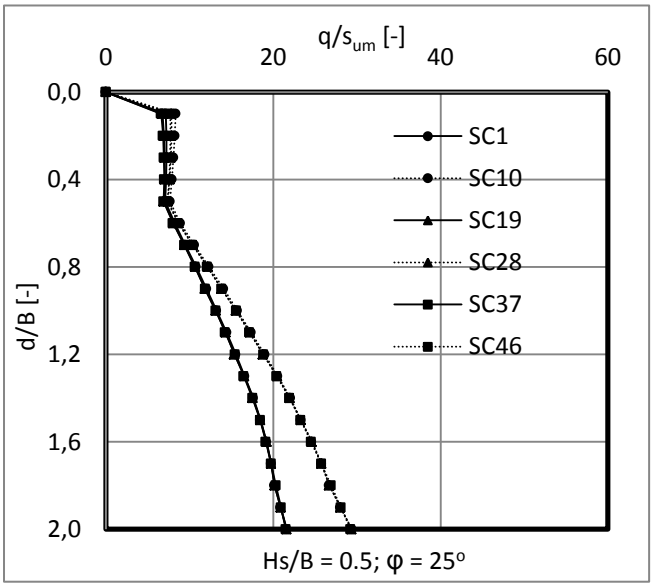

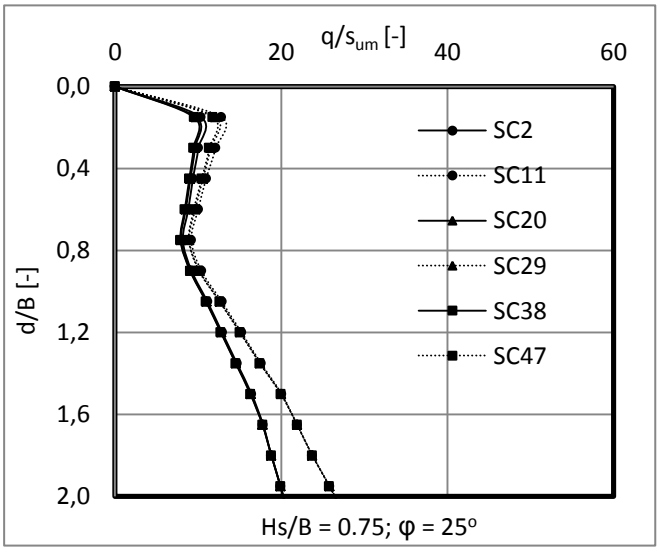

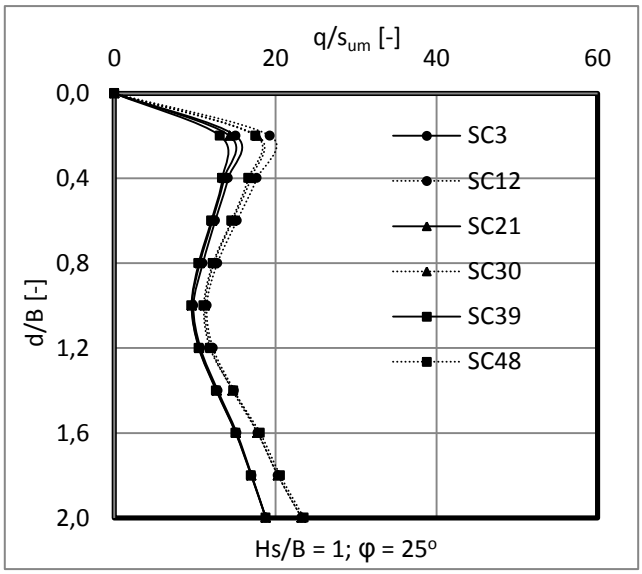

The effect of the friction angle and the sand thickness on the penetration response.

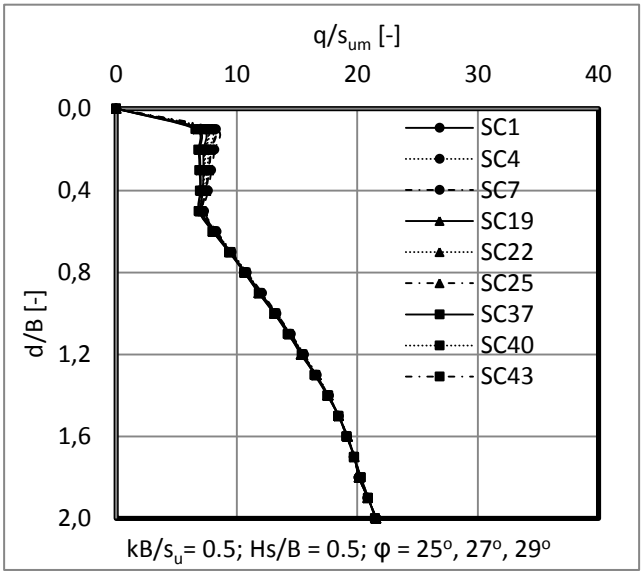

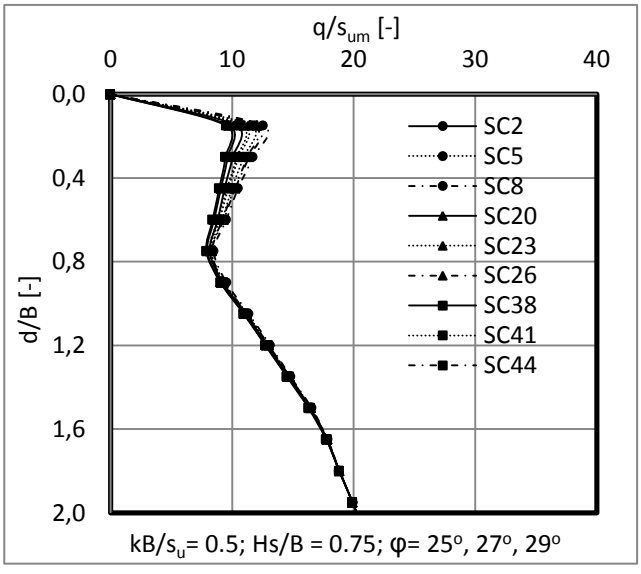

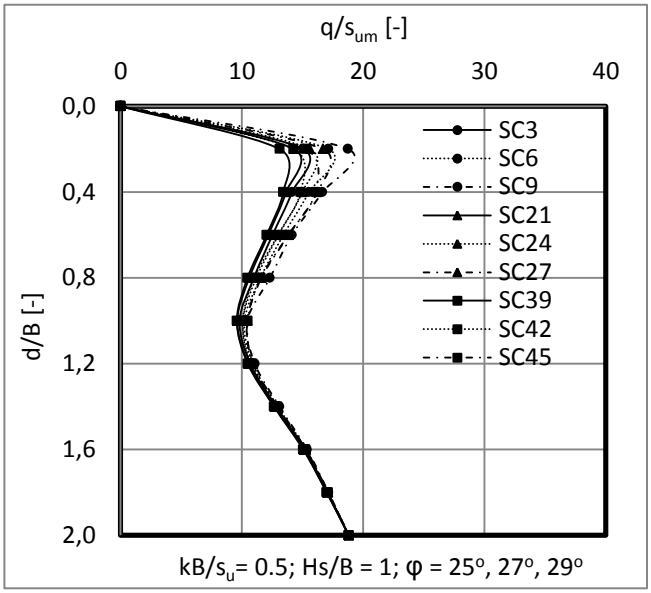
q/s_um [-]
0
10
20
30
40
0,0
0,4
0,8
1,2
1,6
2,0
d/B [-]
SC3
SC6
SC9
SC21
SC24
SC27
SC39
SC42
SC45
kB/s_u= 0.5; Hs/B = 1; φ = 25°, 27°, 29°